Late Triassic to Jurassic Magmatic and Tectonic Evolution of the Intermontane Terranes in Yukon, Northern Canadian Cordillera: Transition from Arc to Syn-Collisional Magmatism and Post-Collisional Lithospheric Delamination

Maurice Colpron[1], Patrick J. Sack[1], James L. Crowley[2], Luke P. Beranek[3], and Murray M. Allan[4†]

[1] Yukon Geological Survey, PO Box 2703 (K14), Whitehorse, Yukon, Canada, Y1A 2C6.

[2] Boise State University, 1910 University Drive, Boise, Idaho, USA, 83725-1535.

[3] Memorial University of Newfoundland, St. John's, Newfoundland and Labrador, Canada, A1B 3X5.

[4] Mineral Deposit Research Unit, The University of British Columbia, Department of Earth, Ocean and Atmospheric Sciences, 2020 – 2207 Main Mall, Vancouver, British Columbia, Canada, V6T 1Z4.

Corresponding author: Maurice Colpron (maurice.colpron@yukon.ca)

[†] currently at: Teck Resources Limited, 3300-550 Burrard St., Vancouver, British Columbia, Canada, V6C 0B3.

Key Points:

- End-on latest Triassic to Early Jurassic arc–continent collision in the northern Cordillera
- Crustal thickening and syn-collisional magmatism north of Stikine arch linked by transform faults to retreating Hazelton slab to the south
- Southward slab retreat and transform faults result in entrapment of the Cache Creek terrane

Abstract

End-on arc collision and onset of the northern Cordilleran orogen is recorded in Late Triassic to Jurassic plutons in the Intermontane terranes of Yukon, and in development of the synorogenic Whitehorse trough (WT). A synthesis of the extensive dataset for these plutons supports interpretation of the magmatic and tectonic evolution of the northern Intermontane terranes. Late Triassic juvenile plutons that locally intrude the Yukon-Tanana terrane represent the northern extension of arc magmatism within Stikinia. Early Jurassic plutons that intrude Stikinia and Yukon-Tanana terranes were emplaced during crustal thickening (200-195 Ma) and subsequent exhumation (190-178 Ma). The syn-collisional magmatism migrated to the south and shows increasing crustal contributions with time. This style of magmatism in Yukon contrasts with coeval, juvenile arc magmatism in British Columbia (Hazelton Group), that records southward arc migration in the Early Jurassic. Exhumation and subsidence of the WT in the north were probably linked to the retreating Hazelton arc by a sinistral transform. East of WT, Early Jurassic plutons intruded into Yukon-Tanana record continued arc magmatism in Quesnellia. Middle Jurassic plutons were intruded after final enclosure of the Cache Creek terrane and imbrication of the Intermontane terranes. The post-collisional plutons have juvenile isotopic compositions that, together with stratigraphic evidence of surface uplift, are interpreted to record asthenospheric upwelling and lithospheric delamination. A revised tectonic model proposes that entrapment of the Cache Creek terrane was the result of Hazelton slab rollback and development of a sinistral transform fault system linked to the collision zone to the north.

1 Introduction

Crustal growth at convergent margins is generally thought to occur through accretion of juvenile arc crust and/or addition of magmatic material to the edge of a craton (e.g., Rudnick, 1995). Arc–continent collision zones are thus major sites for crustal growth through time (e.g., Brown et al., 2011). Arc accretion generally leads to development of an accretionary orogen, associated magmatism and basin(s) (e.g., Cawood et al., 2009; Draut & Clift, 2012). The evolution of arc–continent collision zones is generally complex and shows a wide-range of variations depending on configuration of continental and arc crusts, and angle and rates of convergence (Brown et al., 2011). There is no simple model that explains the variations observed in modern and ancient arc–continent collisions.

In western North America, the development of the northern Cordilleran accretionary orogen began with collision of early Mesozoic peri-Laurentian arcs with the continental margin in latest Triassic to Early Jurassic (Monger & Nokleberg, 1996; Monger & Price, 2002; Nelson et al., 2013; Colpron et al., 2015; George et al., 2021). Initial accretion involved the Intermontane terranes (Fig. 1), which occupy the core of the orogen in Canada and include a series of magmatic arcs (Stikinia, Quesnellia, Yukon-Tanana), marginal ocean basins (Slide Mountain) and accretionary complexes (Cache Creek) that evolved at the western edge of the Laurentian plate (ancestral North America) between mid-Paleozoic and early Mesozoic (Monger et al., 1982; Colpron et al., 2007; Nelson et al., 2013). The Late Triassic magmatic arcs of Quesnellia and Stikinia are generally interpreted to have formed part of a contiguous arc system that was duplicated during Early to Middle Jurassic accretion, either as a consequence of strike-slip faulting (Wernicke & Klepacki, 1988) or oroclinal bending (Nelson & Mihalynuk, 1993; Mihalynuk et al., 1994, 2004). This resulted in entrapment of the Cache Creek terrane – the

accretionary complex and related arc and oceanic rocks that developed in the forearc of Stikinia and Quesnellia (Monger, 1977; Travers, 1978; Monger et al., 1982). There is increasing evidence that arc–continent collision and crustal thickening first occurred in the latest Triassic – earliest Jurassic in the northern Intermontane terranes north of the Stikine arch (Fig. 1) and was followed by Early Jurassic exhumation of Stikinia and the Yukon-Tanana terranes in Yukon. Evidence of latest Triassic to Early Jurassic tectonism include: 1) folding of Late Triassic strata and development of regional Early Jurassic unconformities (Greig & Gehrels, 1995; Brown et al., 1996; Greig, 2014; George et al., 2021); 2) ca. 205-195 Ma amphibolite-facies regional metamorphism in rocks of the Yukon-Tanana terrane (Clark, 2017; Gaidies et al., 2021); and 3) widespread Early Jurassic mica cooling ages in metamorphic rocks of the Yukon-Tanana terrane (Colpron et al., 2015). The Early to Middle Jurassic Whitehorse trough was developed as a synorogenic piggyback basin atop this nascent orogen, and its sediments were sourced from locally exhumed rocks of Stikinia and Yukon-Tanana terranes and their contained intrusions (Colpron et al., 2015; van Drecht, 2019). Initial encroachment of the accreted terranes onto the western North American margin is constrained by Early Jurassic syn-tectonic, Alaskan-type intrusions in Quesnellia (Murphy et al., 1995; Nixon et al., 1997, 2020) and initial subsidence of the Alberta foreland basin that contains strata with syn-depositional detrital zircons (Sinemurian-Toarcian; Asgar-Deen, 2003; McCartney, 2012; Pană et al., 2018). The demise of the early Mesozoic peri-Laurentian arcs and initial growth of the Cordilleran orogen in the latest Triassic to Early Jurassic was apparently related to the westward drift of the North American continent during breakup of the supercontinent Pangea and subsequent opening of the central Atlantic Ocean (Coney, 1972; Dickinson, 2004; Monger & Gibson, 2019).

Between Late Triassic and Late Jurassic, the evolution of this arc–continent collision was accompanied by intrusion of granitoid plutons (Armstrong, 1988; Wheeler & McFeely, 1991; Woodsworth et al., 1991; Nelson et al., 2013). The Late Triassic to Early Jurassic plutons broadly form two parallel belts that extend the length of Quesnellia and Stikinia in British Columbia and converge in the Yukon-Tanana terrane of central Yukon and eastern Alaska (Figs. 1 and 2). They have generally been considered arc plutons related to coeval juvenile volcanism in Stikinia and Quesnellia (e.g., Dostal et al., 2001; Logan & Mihalynuk, 2014), but plutons in Yukon have received limited attention to date. In this contribution, we present a synthesis and interpretation of the extensive dataset compiled by Sack et al. (2020) in their *Atlas of Late Triassic to Jurassic plutons in the Intermontane terranes of Yukon*. The Atlas presents a systematic description of most Late Triassic to Jurassic plutons exposed between latitudes 60°N and 63°15'N in southern Yukon (Fig. 2). This dataset is anchored on 35 high-precision U-Pb zircon dates and associated geochemical and isotopic data that allow for a detailed analysis of magmatism within the arc–continent collision zone in Yukon. The integrated dataset provides means to refine terrane boundaries in Yukon, more specifically between Stikinia and Quesnellia, and to test current tectonic models. Our analysis shows that Late Triassic to Jurassic plutons in Yukon record a transition from arc, to syn- and post-collision magmatism that is distinct from continued, juvenile arc magmatism in British Columbia (George et al., 2021). Together with recent studies of Late Triassic to Jurassic sedimentary and volcanic strata in British Columbia and Yukon (Colpron et al., 2015; van Drecht, 2019; George et al., 2021; Nelson et al., 2022) our synthesis provides the basis for a revised tectonic model for the early Mesozoic development of the northern Cordilleran accretionary orogen. Our model provides another example for the

evolution of an ancient arc–continent collision and subsequent development of an accretionary orogen.

2 Accretionary history of the Intermontane terranes

The Intermontane terranes are primarily composed of a series of superposed magmatic arc successions ranging from Late Devonian to Early Jurassic. The oldest of the Intermontane terranes in Yukon is the Yukon-Tanana terrane, which includes three arc successions of Late Devonian to middle Permian age (Finlayson, Klinkit and Klondike assemblages) that were developed on top of a pre-Devonian metasedimentary succession (Snowcap assemblage; Mortensen & Jilson, 1985; Mortensen, 1992; Colpron et al., 2006a, 2007). The Snowcap assemblage is interpreted as a rifted fragment of the western Laurentian continental margin (Piercey & Colpron, 2009). Arc successions in the Yukon-Tanana terrane comprise two main pulses of felsic magmatism at 365-330 Ma and 264-254 Ma, and an intervening mafic volcanic succession (Colpron et al., 2006a; Nelson et al., 2006). The Mississippian to early Permian mafic volcanic and carbonate rocks of the Klinkit assemblage are correlated with Paleozoic arc sequences of Quesnellia in British Columbia (Lay Range and Harper Ranch assemblages; Ferri, 1997; Beatty et al., 2006), leading to the interpretation that Yukon-Tanana is locally the basement to Mesozoic Quesnellia (Simard et al., 2003; Nelson & Friedman, 2004; Roots et al., 2006; Colpron et al., 2007; Nixon et al., 2020).

Arc development in the Yukon-Tanana terrane was coeval with opening of the Slide Mountain back-arc ocean between Late Devonian and early Permian (Mortensen, 1992; Creaser et al., 1999; Nelson et al., 2006; Colpron et al., 2007; Colpron & Nelson, 2009). Closure of the Slide Mountain ocean is recorded in ca. 270-255 Ma eclogite at the eastern edge of Yukon-Tanana terrane (e.g., Creaser et al., 1997a; Erdmer et al., 1998; Petrie et al., 2016; Gilotti et al.,

2017) and ca. 264-254 Ma magmatism of the Klondike assemblage (Mortensen, 1990, 1992). By Middle to Late Triassic, siliciclastic rocks, derived in part from the Yukon-Tanana terrane and the Laurentian craton, overlap Yukon-Tanana, Quesnellia, Slide Mountain and the western North American margin and indicate that the Slide Mountain Ocean had closed by that time (e.g., Unterschutz et al., 2002; Beranek & Mortensen, 2011).

The oldest rocks in Stikinia are also Paleozoic arc successions; these are distinctly more primitive in character and of uncertain relationship with coeval arc magmatism in the Yukon-Tanana terrane. In northwest British Columbia, the Stikine assemblage comprises Devonian to Permian volcanic and volcaniclastic rocks of primitive arc affinity, associated Late Devonian to Early Mississippian calc-alkaline plutons, and Carboniferous to lower Permian (Cisuralian) limestone (Monger, 1977; Logan et al., 2000; Gunning et al., 2006). Correlative rocks in southern Yukon include metamorphosed volcanic, volcaniclastic, and minor carbonate rocks of the Pennsylvanian-Permian Takhini assemblage (Hart, 1997). Takhini metabasites have the geochemical characteristics of primitive island arc tholeiites (Bordet et al., 2019). In central Yukon, east of Carmacks (Fig. 2), the Boswell assemblage includes: 1) a lower unit of Upper Devonian to Lower Mississippian basalt (normal and enriched mid-ocean ridge basalt [MORB]) and limestone; and 2) an upper unit of Upper Mississippian to lower Permian arc volcanic, volcaniclastic, and sedimentary rocks (including Pennsylvanian-Permian fossiliferous limestone and Pennsylvanian tonalite and rhyolite; Simard, 2003; Simard & Devine, 2003; Colpron, 2011). These rocks were previously assigned to Quesnellia (e.g., Gordey & Makepeace, 2001; Colpron, 2011) but are considered part of Stikinia in this paper for reasons discussed below.

Volcanic components of the Upper Triassic successions of Quesnellia and Stikinia are predominantly augite-phyric basalt and andesite with primitive arc geochemical and isotopic

signatures (Dostal et al., 1999; Bordet et al., 2019). The similar Upper Triassic stratigraphy and petrogenesis in these two terranes suggest that they formed parts of a common Late Triassic arc system that is now duplicated as the result of Early Jurassic oroclinal bending (Mihalynuk et al., 1994) and/or strike-slip faulting (Wernicke & Klepacki, 1988). In British Columbia, Upper Triassic to Lower Jurassic rocks of Stikinia and Quesnellia occur on either side of the Cache Creek terrane, the accretionary complex that developed adjacent to the arc terranes (Fig. 1; Monger, 1977; Travers, 1978). In southern Yukon, the Cache Creek terrane terminates near 61°N latitude (Fig. 2; Bickerton et al., 2020) and similar Upper Triassic strata of Stikinia occur continuously around its northern end.

The Cache Creek terrane includes fragments of primitive arc crust, seamounts with Pennsylvanian-Permian limestone caps (locally with early Permian fusilinids of Tethyan affinity; Monger & Ross, 1971; Ross & Ross, 1983), extensive late Permian (Lopingian) to Middle Triassic supra-subduction zone ophiolites, pelagic sedimentary rocks, and synorogenic clastic rocks with protolith ages ranging from Mississippian to Early Jurassic (Monger, 1977; Cordey et al., 1991; Mihalynuk et al., 2004; McGoldrick et al., 2017; Cordey, 2020).

The Lower to Middle Jurassic clastic sedimentary rocks of the Whitehorse trough (Laberge Group) overlap Stikinia and Cache Creek terranes in Yukon and northern British Columbia (Wheeler, 1961; Hart, 1997; Mihalynuk et al., 1999; English et al., 2005; Colpron et al., 2015). Correlative strata are also locally unconformable on metamorphic rocks of the Yukon-Tanana terrane (Colpron et al., 2015). In British Columbia, coeval volcanic-sedimentary strata in Stikinia south of the Stikine arch (Fig. 1) are assigned to the uppermost Triassic to Middle Jurassic, arc-related Hazelton Group (Tipper & Richards, 1976; Gagnon et al., 2012; Nelson et al., 2018).

183 Late Triassic to Early Jurassic plutons intrude the length of Stikinia and Quesnellia, and
184 the Yukon-Tanana terrane in Yukon and eastern Alaska (Figs. 1 and 2; Woodsworth et al., 1991;
185 Wilson et al., 2015; Colpron et al., 2016a; Cui et al., 2017). These plutons are closely associated
186 with coeval arc volcanic rocks and porphyry Cu-Au(-Mo) deposits in British Columbia (Fig. 1;
187 Mortensen et al., 1995; Nelson et al., 2013; Logan & Mihalynuk, 2014). In Yukon, Late Triassic
188 plutons are inferred to be subvolcanic feeders to basaltic andesite of the Lewes River Group, but
189 the younger, Early Jurassic plutons lack direct association with coeval volcanism, and Lower
190 Jurassic volcanic rocks are limited to local tuff horizons within the Laberge Group (Tempelman-
191 Kluit, 1984, 2009; Hart, 1997; Johannson et al., 1997; Colpron & Friedman, 2008). Detrital
192 zircon ages and clast compositions in strata of the Laberge Group indicate that the Late Triassic
193 to Early Jurassic plutons exposed on the flanks of Whitehorse trough were major, local sediment
194 sources that were exhumed during marine deposition (Dickie & Hein, 1995; Hart et al., 1995;
195 Shirmohammad et al., 2011; Colpron et al., 2015; van Drecht, 2019). The Laberge Group is
196 unconformably overlain by fluvial and lacustrine strata of the Upper Jurassic to Lower
197 Cretaceous Tantalus Formation, which are interpreted to have been deposited in confined
198 intermontane valleys (Tempelman-Kluit, 1984, 2009; Long, 2015).
199 Strata of the Intermontane terranes were folded and imbricated by east-dipping, west-
200 verging thrust faults prior to intrusion of Middle to Late Jurassic plutons (Tipper, 1978;
201 Gabrielse, 1998; Mihalynuk et al., 2004). In Yukon, these plutons define a central belt that
202 stitches Stikinia, Cache Creek, and Whitehorse trough west of the Teslin fault (Fig. 2). Major
203 Jurassic structures include the King Salmon, Nahlin, Wann River, and Llewellyn faults in
204 northern British Columbia (Currie & Parrish, 1993; Gabrielse, 1998; Mihalynuk et al., 1999),
205 and the Needlerock, Tadru, and Yukon River faults in Yukon (Fig. 3; Colpron et al., 2002, 2003;

206 Colpron & Ryan, 2010; Ryan et al., 2013, 2014; Parsons et al., 2018). Metamorphic studies of
207 the Yukon-Tanana terrane in western Yukon and northwestern British Columbia indicate that
208 structural imbrication led to crustal thickening, tectonic burial to depths of 20-30 km, and
209 subsequent exhumation in the Early Jurassic (Berman et al., 2007; Clark, 2017; Dyer, 2020;
210 Gaidies et al., 2021). The Willow Lake fault in central Yukon is a low-angle normal fault
211 inferred to have accommodated part of the Early Jurassic exhumation (Colpron & Ryan, 2010;
212 Knight et al., 2013).

213 The Intermontane terranes and their Late Triassic to Jurassic plutons are dissected by a
214 series of post-accretionary strike-slip faults, including the Late Cretaceous Teslin, d'Abbadie,
215 Big Salmon, and Towhata faults, and the Paleocene Tintina fault (Fig. 2). In seismic and
216 magnetotelluric profiles across southern Yukon (SNORCLE line 3), the Teslin fault appears to
217 be underlain by east-dipping anomalies that project to mid-crustal levels (Cook et al., 2004;
218 Dehkordi et al., 2019). Farther north, in central Yukon, an interpretation of seismic and gravity
219 data across the Intermontane terranes shows the Big Salmon fault as a more significant west-
220 dipping structure that extends to lower crustal levels and is laterally more continuous than the
221 Teslin fault at this latitude (Calvert et al., 2017).

222 In Figure 3, dextral strike-slip displacement has been restored on major Late Cretaceous
223 and Paleocene faults in order to show the configuration of terranes and distribution of Early and
224 Middle Jurassic plutonic suites in Late Jurassic to Early Cretaceous time, after imbrication of the
225 Intermontane terranes and accretion to western North America. This Early Cretaceous
226 palinspastic map provides the framework for the following discussion of Late Triassic to Jurassic
227 magmatism in the Intermontane terranes of Yukon.
228

3 Late Triassic – Jurassic plutonic suites

Extensive studies, summarized in this paper, result in subdivision of the Late Triassic to Jurassic plutons in Yukon into eight plutonic suites based mainly on age (Fig. 4) and composition (Fig. 5), but also to some extent on relationship with their host terrane, and geographic distribution (Figs. 2 and 3; Sack et al., 2020). From oldest to youngest, these suites are:

1. the Late Triassic Pyroxene Mountain (220-214 Ma) and Stikine (217-214 Ma) suites;
2. the latest Triassic to Early Jurassic Minto (205-194 Ma), Lokken (195-184 Ma), Long Lake (188-183 Ma), and Bennett (178-175 Ma) suites;
3. the Middle Jurassic Bryde suite (174-168 Ma) and Late Jurassic McGregor suite (163-146 Ma).

3.1 Methods and dataset

The core of this dataset was acquired during field investigations of 32 plutons between 2014 and 2018, augmented with data collected during previous regional mapping programs (1999-2013; see Sack et al., 2020, for complete sources of data). Of the more than 450 granitoid rock samples collected, 171 were slabbed and stained for petrographic analysis (Appendices 2 and 13 in Sack et al., 2020), including semi-automated estimates of modal abundances of quartz, alkali feldspar, plagioclase and mafic minerals using the ImageJ software (Fig. 5a; Schneider et al., 2012). Thin sections were cut from 209 samples and 204 samples were analyzed for major and trace element geochemistry (Fig. 5b-d; Appendix 8 in Sack et al., 2020). Age ranges for the eight plutonic suites are anchored on 35 high-precision U-Pb zircon dates determined using the

chemical abrasion thermal ionization mass spectrometry (CA-TIMS) method (Fig. 4; Table 1-2 and Appendix 4 in Sack et al., 2020; see also Sack et al., 2022 for one additional sample). Thirty-four of these samples were analyzed at Boise State University (BSU) and one sample at the University of British Columbia (UBC). Most samples analyzed at BSU were first imaged by cathodoluminescence (CL) and analyzed by laser ablation inductively coupled plasma mass spectrometry (LA-ICPMS) before CA-TIMS analysis (Appendix 3 in Sack et al., 2020). Approximately 30 LA-ICPMS spots in each sample were analyzed for U-Pb isotopes and trace element chemistry to characterize the zircon population(s) present. Zircon grains dated by CA-TIMS were selected from the youngest statistically coherent LA-ICPMS population with similar chemical composition and CL response. Inherited cores were encountered in 15 of the 33 samples analyzed and documented by LA-ICPMS (Table 1-2 and Appendix 3 in Sack et al., 2020). The Atlas also reports new $^{40}Ar/^{39}Ar$ dates for hornblende, muscovite, and biotite from 25 samples (Appendix 6 in Sack et al., 2020). Most of the mica dates provide estimates for cooling of these plutons to upper crustal levels (≤300-350°C; Hodges, 2014). A few hornblende dates from Late Triassic intrusions and muscovite dates in the central part of the Late Jurassic McGregor pluton provide the best estimate for crystallization for these plutons.

Whole rock analyses of Rb-Sr and Sm-Nd isotopes were acquired at Carleton University from 30 of the dated samples (Table 1-4 and Appendix 9 in Sack et al., 2020). Zircons from 22 of the samples dated at BSU were also analyzed for Lu-Hf isotopes using the LA-ICPMS laboratory at Memorial University of Newfoundland (MUN; Appendix 10 in Sack et al., 2020). The Hf isotope data were acquired at MUN on the same zircon mounts used at BSU with 40 μm Hf spot analyses located on top of smaller U-Pb ablation pits so the data are as related as possible.

Crystallization pressures were calculated using the Al-in-hornblende geobarometer for 26 samples that contain the required mineral assemblage (Hammarstrom & Zen, 1986; Anderson & Smith, 1995). Electron microprobe analyses of plagioclase and hornblende were performed at UBC (Table 1-3 and Appendix 5 in Sack et al., 2020). Total 1σ errors in pressure generally range from 0.8 to 1.1 kbar, such that all depth estimates quoted in this study have an associated error of ~3-4 km.

3.2 Late Triassic plutonic suites

Late Triassic plutons associated with arc volcanic rocks of Stikinia occur in two main clusters in southern Yukon. South of Whitehorse (Fig. 2), the Stikine suite (217-214 Ma) comprises small monzodiorite, monzonite, and granodiorite plutons (Fig. 5a) that intrude Upper Triassic volcanic and volcaniclastic rocks of Stikinia (Lewes River Group) near its western edge. Uranium-lead zircon CA-TIMS $^{206}Pb/^{238}U$ dates range from 216.48 ± 0.06 to 214.42 ± 0.07 Ma (Fig. 4). The plutons are oxidized, calc-alkaline to high-K calc-alkaline, and mostly metaluminous (Fig. 5c-d). They are isotopically juvenile with εNd_t of +5.2 to +5.3 and $^{87}Sr/^{86}Sr_i$ of 0.7042 to 0.7047 (Figs. 6 and 7). Zircons from the Stikine suite have εHf_t ranging +9.7 to +11.6 (Fig. 6c). No inherited zircon cores were encountered in the Stikine suite. Crystallization pressure estimates were determined from only one pluton (Friday Creek, Fig. 2) and indicate emplacement at 3.1 to 3.5 kbar (emplacement depths of 12-13 km; Fig. 8).

A second cluster of small Late Triassic plutons north of Carmacks (Fig. 2), the Pyroxene Mountain suite (220-214 Ma; Ryan et al., 2013), is not as well studied. They include mainly hornblende gabbro, diorite, and pyroxenite that are generally coarse to very coarse grained. The plutons intrude metamorphic rocks of the Yukon-Tanana terrane northwest of the last exposures of Upper Triassic volcanic rocks of Stikinia (Povoas Formation, Lewes River Group) with which

297 the plutons are inferred to be comagmatic (Tempelman-Kluit, 1984, 2009; Ryan et al., 2013).
298 Similar coarse grained hornblende gabbro and amphibolite also occur within rafts in Early
299 Jurassic plutons of the Minto suite where they intrude Upper Triassic metavolcanic rocks (Ryan
300 et al., 2013). Zircons from plutons of the Pyroxene Mountain suite previously yielded imprecise
301 U/Pb dates between 220 and 211 Ma, but $^{40}Ar/^{39}Ar$ dates from hornblende of the Pyroxene
302 Mountain pluton and amphibolite rafts in Early Jurassic batholiths have a narrower range from
303 218-214 Ma (Sack et al., 2020). A new CA-TIMS date from a Pyroxene Mountain pluton at
304 Mount Nansen, west of Carmacks (Fig. 2; previously dated at ca. 211 Ma by LA-ICPMS;
305 Klöcking et al., 2016), has an age of 216.16 ± 0.07 Ma (Sack et al., 2022) and CA-TIMS analysis
306 of zircon fragments in a mineralized raft at the Carmacks Copper deposit indicate a protolith age
307 of 217.53 ± 0.16 Ma (Kovacs et al., 2020). These results suggest that the Pyroxene Mountain
308 suite is the northern extension of the Stikine suite in central Yukon and that Stikinia is locally
309 anchored on the Yukon-Tanana terrane.

310 3.3 Early Jurassic plutonic suites

311 Early Jurassic granitoid plutons are widespread in southern Yukon, where they occur on
312 either side of Triassic volcanic rocks of Stikinia/Quesnellia, and Jurassic sedimentary strata of
313 the Whitehorse trough (Figs. 2 and 3). Although the earliest phases in some plutons of the Minto
314 suite are latest Triassic (ca. 205-203 Ma), the bulk of these plutons are Early Jurassic (198-195
315 Ma) and assigned to that epoch here for simplicity. The Early Jurassic plutons have a distinct
316 character on either side of the Big Salmon–Teslin fault system (BSTF). West of the BSTF, large
317 batholiths of the Minto (205-194 Ma), Long Lake (188-183 Ma) and Bennett (178-175 Ma)
318 suites intrude the boundary between Stikinia and Yukon-Tanana terranes. They are mainly
319 composed of granodiorite and granite (Fig. 5a-b) with the older Minto suite intruding near the

apex of Late Triassic Stikinia and progressively younger batholiths of the Long Lake and Bennett suites intruding its western edge to the south (Figs. 3 and 4). East of the BSTF, Early Jurassic plutons of the Lokken suite (195-184 Ma) are distinctly more mafic and alkalic (Fig. 5a-b), typically form small plutons, show no systematic age distribution (Figs. 3 and 4), and intrude only the Yukon-Tanana terrane.

3.3.1 *Minto suite*

The Minto suite is predominantly composed of hornblende-biotite granodiorite and subordinate granite, quartz monzonite, and diorite (Fig. 5a-b). Uranium-lead zircon CA-TIMS $^{206}Pb/^{238}U$ dates range mainly from 198.22 ± 0.06 to 194.71 ± 0.07 Ma (Fig. 4). The granodiorite is medium grained equigranular to coarse grained and K-feldspar porphyritic. It is locally foliated or gneissic, but more typically unfoliated. Euhedral magmatic epidote is common in granodiorite of the Minto suite (Sack et al., 2020). Minto suite plutons are generally oxidized, calc-alkaline to high-K calc-alkaline to weakly shoshonitic, and predominantly peraluminous (Fig. 5). Whole rock isotopic data range from -3.6 to +1.3 for εNd_t, and 0.7047 to 0.7062 for $^{87}Sr/^{86}Sr_i$; εHf_t in zircon range from +0.5 to +10.9 (Figs. 6 and 7).

The K-feldspar megacrystic border phase of the Tatchun batholith yielded an older CA-TIMS $^{206}Pb/^{238}U$ date of 203.32 ± 0.06 Ma (Fig. 4). Although this is the only precisely dated latest Triassic phase in this study, the presence of 205-203 Ma zircon antecrysts in the Granite Mountain batholith (Sack et al., 2020; Kovacs et al., 2020) and an imprecise date of 204.9 ± 3.3 Ma from the Pelly pluton (Knight et al., 2013) suggest that this early phase may be more widespread than presently documented in the Minto suite. Inherited zircons are documented in the Granite Mountain, Minto, and Tatchun plutons (Fig. 3; Sack et al., 2020; Kovacs et al., 2020). They show a bimodal age distribution with peaks in the Late Triassic (ca. 213 Ma) and

Mississippian (ca. 344-327 Ma; Fig. 9a). Late Triassic zircons have εHf_t of +3.2 to +6.0 and Mississippian zircons have εHf_t of +3.7 to +10.9.

Crystallization pressure estimates using the Al-in-hornblende method were determined for the Granite Mountain, Minto, Walhalla, and Tatchun plutons (McCausland et al., 2002; Tafti, 2005; Topham et al., 2016; Sack et al., 2020). Plutons west of the Teslin fault have emplacement pressures of 4.8 to 5.9 kbar, whereas samples from the Tatchun batholith to the east of the fault consistently yield higher pressures of 6.4 to 6.8 kbar (Fig. 8). These values suggest emplacement depths of 15-25 km for the Granite Mountain, Minto, and Walhalla plutons, and of 21-30 km for the Tatchun batholith. These emplacement pressures are consistent with upper greenschist to amphibolite facies metamorphism of host rocks for these plutons (Read et al., 1991).

Plutons of the Minto suite contain a belt of Cu-Ag-Au deposits (Minto, Carmacks Copper and Stu; Fig. 2). The mineralization is dated at ca. 217-213 Ma and occurs in variably metamorphosed and migmatized rafts and xenoliths of foliated intermediate to mafic meta-igneous rocks of probable Stikine suite affinity, enveloped within massive plutonic phases of the Minto suite (Kovacs et al., 2020; Sack et al., 2020).

3.3.2 *Long Lake suite*

The Long Lake suite is primarily represented by the Aishihik batholith, Big Creek pluton, and southwest portion of the Granite Mountain batholith (Figs. 2 and 3); it ranges from tonalite-granodiorite to granite and syenite (Fig. 5a-b). The Aishihik batholith comprises two main phases that are close in age and locally intermixed. The older phase is composed of hornblende (± biotite) granodiorite to tonalite. It is fine to medium grained, equigranular to locally K-feldspar porphyritic, and melanocratic with hornblende typically more abundant than biotite. The younger phase comprises coarser grained granodiorite and granite characterized by coarse, grey

366 quartz glomerocrysts. The rock is equigranular to K-feldspar porphyritic, generally leucocratic
367 with mainly biotite and rare hornblende, and local muscovite. Granite phases are commonly
368 associated with aplite dikes and pegmatite pods. The southwest portion of the Granite Mountain
369 batholith is composed mainly of granodiorite and minor granite. Distinctive very coarse grained,
370 hornblende-K-feldspar monzonite and syenite comprise the main phase in the Big Creek pluton.
371 Zircon CA-TIMS $^{206}Pb/^{238}U$ dates range from 187.46 ± 0.07 to 182.83 ± 0.05 Ma (Fig.
372 4). In the Aishihik batholith, the 'older', melanocratic granodiorite phase (Aishihik 1 in Table 1-2
373 of Sack et al., 2020) yielded dates ranging from 186.22 ± 0.10 to 183.28 ± 0.07 Ma, while the
374 'younger' granite phase (Aishihik 2) is dated at 184.06 ± 0.06 Ma, consistent with intermingling
375 of these phases observed in outcrop.
376 Granodiorite and granite of the Long Lake suite are oxidized, calc-alkaline to high-K
377 calc-alkaline, and mainly peraluminous, whereas syenite of the Big Creek pluton is oxidized,
378 high-K calc-alkaline to shoshonitic, and metaluminous (Fig. 5). Plutons of the Long Lake suite
379 have the most evolved isotopic signature of all Jurassic intrusions in Yukon with $^{87}Sr/^{86}Sr_i$ of
380 0.7051 to 0.7065, εNd_t of -5.9 to -1.5, and εHf_t in zircon of -5.8 to +6.4 (Figs. 6 and 7).
381 Inherited zircon cores were documented in 7 of the 10 samples analyzed from plutons of
382 the Long Lake suite. The dominant population (53% of analyses) includes cores with dates
383 ranging from 209 to 193 Ma that define a sharp peak at ca. 199 Ma (Fig. 9b). Older zircon cores
384 are present but form more subdued populations compared to those in the Minto suite. Six cores
385 yielded Late Triassic dates (233 to 213 Ma), 4 are Permian (275-250 Ma), 10 are Mississippian
386 (353-324 Ma), and 5 are Late Devonian (378-374 Ma; Fig. 9b). The latest Triassic to Early
387 Jurassic zircons have εHf_t of -6.0 to +7.2, the Late Triassic zircons εHf_t of +3.0 to +10.1, the
388 Permian zircons εHf_t of -15.3, and Devonian-Mississippian zircons εHf_t of -14.3 to +12.1.

Aluminum-in-hornblende pressures were calculated for 7 samples from the Aishihik batholith (Fig. 2) and range from 2.3 to 6.0 kbar, indicating emplacement depths of 9 to 23 km (Fig. 8; Sack et al., 2020). Previous Al-in-hornblende pressures for the southwest Granite Mountain batholith range from 4.4 to 4.7 kbar (McCausland et al., 2002).

3.3.3 *Bennett suite*

The Bennett suite includes much of the Bennett and Alligator Lake plutons south of Whitehorse in Yukon (Fig. 2); a trend of plutons from this suite extends into northern British Columbia west of Atlin (Fig. 3; Mihalynuk et al., 1999). The Bennett suite is composed of K-feldspar porphyritic granodiorite and equigranular monzodiorite and diorite that are locally weakly foliated (Fig. 5a). The groundmass in the granodiorite is generally fine grained with granophyric or graphic textures, suggesting emplacement at shallow depth and/or a water-saturated magma (Sack et al., 2020). A sample of the Bennett Lake batholith has a CA-TIMS $^{206}Pb/^{238}U$ date of 178.18 ± 0.06 Ma (Fig. 4). Previous dates from the Bennett suite suggest it may range as young as ca. 175 Ma (Hart, 1995). The rocks are oxidized, subalkaline diorite to granite in composition (SiO_2 62-70%; Fig. 5b). They are calc-alkaline to high-K calc-alkaline and peraluminous (Fig. 5c-d) and have some of the most enriched trace element concentrations of all Early Jurassic plutons (Sack et al., 2020). Two samples from the Bennett suite have moderately evolved isotopic signatures with $^{87}Sr/^{86}Sr_i$ of 0.7052 and 0.7053, and εNd_t of -2.5 (Figs. 6 and 7). No inheritance was documented in the limited LA-ICPMS U-Pb analyses from the Bennett suite. Two samples were analyzed for Al-in-hornblende barometry. One sample has total Al (Al^{TOT}) too low to yield meaningful results, while a crystallization pressure of 3.5 kbar from the other sample suggests emplacement at depths ≤13 km (Fig. 8).

411 3.3.4 *Lokken suite*

412 The Lokken suite is a belt of small plutons intruding metamorphic rocks of the Yukon-
413 Tanana terrane east of the BSTF in southern Yukon (Figs. 2 and 3). The Lokken suite extends
414 south into northernmost British Columbia, where it forms parts of the large, composite
415 Coconino–Simpson Peak–Nome Lake batholith (Fig. 3; Roots et al., 2006; Cui et al., 2017; Han
416 et al., 2020). The plutons are composed mainly of mesocratic, medium grained, equigranular
417 hornblende-biotite-clinopyroxene monzodiorite, monzonite, diorite, and granodiorite (Fig. 5a-b).
418 Zircon CA-TIMS $^{206}Pb/^{238}U$ dates range from 194.67 ± 0.05 to 184.21 ± 0.05 Ma (Fig. 4). K-
419 feldspar porphyritic monzonite and granodiorite also occur in some of the younger plutons (e.g.,
420 ca. 188-184 Ma Logjam and Two Ladder plutons). Mafic to ultramafic gabbro, pyroxenite, and
421 variably serpentinized dunite locally occur as border phases in some plutons (e.g., Roots et al.,
422 2004). Hornblende-clinopyroxene syenite is present in plutons intruding the Yukon-Tanana
423 terrane northeast of the Tintina fault (e.g., Banana pluton, Figs. 2 and 3). Older phases of the
424 Lokken suite are locally foliated and local development of myrmekitic texture suggests
425 subsolidus metasomatism and/or deformation.

426 Plutons of the Lokken suite are oxidized, subalkaline to alkaline, high-K calc-alkaline to
427 shoshonitic, and metaluminous, and occupy fields distinct from other suites on Figure 5. They
428 have whole rock isotopic data ranging from 0.7044 to 0.7059 for $^{87}Sr/^{86}Sr_i$ and -4.3 to -0.6 for
429 εNd_t; εHf_t in zircon range from -2.9 to +9.3 (Figs. 6 and 7). Inherited zircon cores were
430 documented in 3 samples from the youngest part of the Lokken suite (<186 Ma; Fig. 3). Only 12
431 analyses were acquired from these samples (Fig. 9c), of which 5 have dates ranging ca. 202-196
432 Ma, two are Late Triassic (ca. 235 and 226 Ma) and two are Mississippian (ca. 354 and 341 Ma).
433 Precambrian cores (n = 3) with dates of ca. 2285, 1698 and 605 Ma were analyzed from the two

youngest plutons in the suite, the ca. 184 Ma Logjam and Sawtooth plutons (Figs. 2 and 3). Inherited cores with Late Triassic dates have εHf_t of +9.2 and +11.6 (Fig. 9).

Only two samples of the Lokken suite had the suitable assemblage for Al-in-hornblende geobarometry. The ca. 192 Ma Lokken and Macmillan Range plutons have calculated pressures of 3.1 and 2.6 kbar, respectively, indicating emplacement at depths of ~10-12 km (Fig. 8).

3.4 Middle to Late Jurassic plutonic suites

The Middle Jurassic Bryde suite occurs along the central axis of the Intermontane terranes, immediately west of the BSTF, and in between the two main belts of Early Jurassic plutons (Figs. 2 and 3). Plutons of the Bryde suite are relatively sparse in southern Yukon but form large batholiths in northern British Columbia, where they are assigned to the Fourth of July suite (Figs. 2 and 3; Mihalynuk et al., 1999). They intrude Stikinia and Cache Creek terranes, and the overlapping Early to Middle Jurassic Whitehorse trough, and postdate the Jurassic southwest-verging structural imbrication of these tectonic elements (Mihalynuk et al., 2004; Bickerton et al., 2020).

Plutons of the Bryde suite are composed of hornblende-clinopyroxene-biotite syenite, monzonite, granodiorite, tonalite, and diorite (Fig. 5a-b). Zircon CA-TIMS $^{206}Pb/^{238}U$ dates for 3 of 4 samples analyzed have a narrow range of 173.44 ± 0.05 to 171.62 ± 0.05 Ma (Fig. 4). The Michie pluton, east of Whitehorse, is younger with a date of 168.09 ± 0.05 Ma (Figs. 2, 3 and 4). The rock varies from fine to coarse grained, to porphyritic and locally pegmatitic, and from leucocratic to melanocratic. Plutons of the Bryde suite are generally reduced, subalkaline to alkaline, calc-alkaline to high-K calc-alkaline, and straddle the metaluminous and peraluminous fields (Fig. 5). They have relatively juvenile isotopic signatures with $^{87}Sr/^{86}Sr_i$ of 0.7040 to 0.7050, and εNd_t of +0.5 to +3.5 (Figs. 6 and 7). Zircon εHf_t form two clusters with samples from

457 the ca. 173-172 Ma Teslin Crossing and Fourth of July plutons yielding juvenile εHf_t values of
458 +4.7 to +8.5, whereas the younger, ca. 168 Ma Michie pluton has lower εHf_t values of +0.8 to
459 +4.0 (Fig. 6c). No inheritance was documented in the 4 samples that were analyzed. A single
460 sample from the northern tip of the Fourth of July batholith contained the suitable assemblage for
461 Al-in-hornblende geobarometry. However, the very low Al^{TOT} in this sample precluded
462 calculation of reliable pressure estimate (Fig. 8). Harris et al. (2003) reported Al-in-hornblende
463 pressures ≤3.1 kbar from the Fourth of July batholith in northern British Columbia.
464 A single Late Jurassic pluton, the McGregor batholith, intrudes the Boswell assemblage
465 between the Teslin and Towhata faults (Fig. 2). It comprises two phases: 1) an older phase of
466 hornblende-biotite granodiorite and granite; and 2) a younger, central phase of two-mica
467 granodiorite and tonalite (Sack et al., 2020). The older granodiorite is medium to coarse grained
468 and commonly K-feldspar porphyritic. Medium grained, equigranular granodiorite is locally
469 present, and a foliation is developed locally along the pluton margins. The two-mica (biotite-
470 muscovite) phase is generally fine to medium grained and equigranular, but also locally K-
471 feldspar porphyritic.
472 Zircon CA-TIMS $^{206}Pb/^{238}U$ dates for 3 samples of the early granodiorite phase of the
473 McGregor batholith range from 163.42 ± 0.05 to 161.16 ± 0.05 Ma (Fig. 4). Zircon from the
474 younger, central phase of two-mica granodiorite yielded a scatter of U-Pb LA-ICPMS dates
475 between ca. 172-136 Ma, including high-U zircon, which precluded precise estimate of its
476 crystallization age (Sack et al., 2020). A muscovite $^{40}Ar/^{39}Ar$ date of 146.8 ± 0.9 Ma provides a
477 minimum age for the two-mica phase of the McGregor batholith. Both phases are reduced,
478 subalkaline, high-K calc-alkaline and peraluminous (Fig. 5). Isotopic data were only collected
479 from the older granodiorite phase of the McGregor batholith. Whole rock $^{87}Sr/^{86}Sr_i$ values for 2

480 samples are 0.7055, and εNd_t are -0.1 and +0.7; εHf_t in zircon range from +0.8 to +4.2 (Figs. 6
481 and 7).

482 Inherited zircon cores were documented in one sample of ca. 161 Ma granodiorite from
483 the McGregor batholith. Twelve of the sixteen spots analyzed have dates ranging from 208 to
484 187 Ma, defining a peak at ca. 199 Ma (Fig. 9d). The remaining 4 analyses are Carboniferous
485 with dates of 322 to 312 Ma. Early Jurassic cores have εHf_t of +3.2 to +4.7 and Mississippian
486 cores have εHf_t of +7.0 to +11.0. Two samples of early granodiorite from the McGregor
487 batholith were analyzed for Al-in-hornblende geobarometry and yielded pressures of 4.5 and 5.3
488 kbar (emplacement depths of ~17-20 km; Fig. 8).

489 **4 Magmatic evolution and tectonic settings**

490 The Late Triassic to Jurassic plutons in south-central Yukon were intruded during
491 progressive arc–continent collision and accretion of the Intermontane terranes in the early
492 Mesozoic; they record distinct steps in the transition from arc to syn- and post collisional
493 magmatism.

494 4.1 Late Triassic Stikine–Lewes River arc

495 The Late Triassic (ca. 217-214 Ma) plutons of the Stikine suite intrude comagmatic,
496 Upper Triassic (Carnian-Norian) volcanic and volcaniclastic rocks of the Povoas formation
497 (Lewes River Group, Stikinia) in southern Yukon (Fig. 2). Stikine suite rocks have
498 metaluminous, calc-alkaline compositions and juvenile isotopic signatures (average εNd_t +5.3;
499 εHf_t in zircon of +10.0; Fig. 6) that are consistent with the primitive arc tholeiite to calc-alkaline
500 basalt compositions of the Povoas formation (average εNd_t +7.5; εHf_t +7.3; Bordet et al., 2019).
501 These data support correlation with the Stuhini–Takla groups and related Late Triassic plutons in

British Columbia (average εNd_t +7.5; Dostal et al., 1999), and the concept that these formed parts of a continuous Late Triassic arc system (e.g., Mihalynuk et al., 1994, 1999; Dostal et al., 1999). The Late Triassic gabbro and pyroxenite of the Pyroxene Mountain suite (best ages ca. 218-214 Ma) are the northern extension of the Stikine suite in central Yukon (Fig. 2; Tempelman-Kluit, 1984, 2009; Ryan et al., 2013). The Pyroxene Mountain suite intrudes the Yukon-Tanana terrane north of Carmacks, suggesting that the northern end of the Late Triassic arc of Stikinia was locally anchored on Yukon-Tanana basement. The ca. 215-212 Ma Taylor Mountain batholith and related plutons of east-central Alaska also intrude the Yukon-Tanana terrane and likely represent the northernmost expression of Stikine arc magmatism (Fig. 1; Dusel-Bacon et al., 2015).

4.2 Early Jurassic syn-collisional magmatism

The style of magmatism in the northern Intermontane terranes of Yukon changed profoundly in the latest Triassic to Early Jurassic, from juvenile intra-oceanic arc to a spatial-temporal sequence of syn-collisional pluton clusters. These plutons were intruded after crustal thickening and burial of the Yukon-Tanana terrane was initiated at ca. 205-200 Ma (Clark, 2017; Kovacs et al., 2020) and during the following phase of exhumation recorded along the flanks of the Whitehorse trough. Crustal thickening was accommodated along a series of southwest-verging shear zones and thrust faults, of which the Needlerock, Tadru, Yukon River, and Reindeer faults are inferred remnants (Fig. 3; Colpron et al., 2002, 2003; Ryan et al., 2013, 2014; Parsons et al., 2018). This latest Triassic to Early Jurassic orogenic activity is inferred to record the initiation of the northern Cordilleran orogen (Colpron et al., 2015).

523 4.2.1 *West of the BSTF*

524 Plutons intruding Stikinia and Yukon-Tanana terranes west of the BSTF form large
525 batholiths of generally peraluminous, calc-alkaline to shoshonitic compositions with more
526 evolved isotopic signatures (εNd_t -5.9 to +1.3; zircon εHf_t -6.0 to +10.3; Fig. 6). In southern
527 Yukon, the locus of magmatism migrated southward through the Early Jurassic, with the older
528 Minto suite (ca. 205-194 Ma) in the north and progressively younger plutons of the Long Lake
529 (ca. 188-183 Ma) and Bennett suites (ca. 178-175 Ma) to the south (Figs. 3 and 4). Early Jurassic
530 plutons west of the BSTF also show progressively more evolved isotopic signatures through
531 time, with the Minto suite yielding near chronditic εNd_t (average of -0.4) compositions and the
532 younger Long Lake and Bennett suites having more evolved εNd_t averages of -3.5 and -2.5,
533 respectively (Fig. 6b). Similar patterns are apparent in $^{87}Sr/^{86}Sr_i$ (Fig. 6a) and εHf_t in zircon (Fig.
534 6c). This progressive shift to more evolved isotopic signatures indicates an increase in crustal
535 interaction through time. Incorporation of older crustal components (e.g., Snowcap assemblage;
536 Piercey & Colpron, 2009) into the Early Jurassic magma is also reflected in the relative
537 abundance of inherited zircon cores in plutons of the Minto and Long Lake suites (Figs. 3 and 9).
538 Plutons of the Minto suite were emplaced in the mid- to lower crust during peak regional
539 metamorphism, and local development of a solid-state foliation in early phases suggest syn-
540 tectonic intrusion. They have Al-in-hornblende crystallization pressures of ~5-7 kbar (~20-25
541 km; Fig. 8) that are consistent with the common occurrence of magmatic epidote in these plutons
542 (Zen and Hammarstrom, 1984; Sack et al., 2020). Although the presence of magmatic epidote
543 and the Al-in-hornblende geobarometer have been questioned as reliable indicators for depth of
544 emplacement (see Schmidt and Poli, 2004, for discussion), regional metamorphic studies of the
545 Yukon-Tanana terrane in western Yukon indicate peak pressures in the Early Jurassic (4-9 kbar,

546 ca. 195-188 Ma; Berman et al., 2007; Clark, 2017; Gaidies et al., 2021) that are broadly
547 consistent with Al-in-hornblende pressures from Minto suite plutons (Fig. 10a). In particular,
548 kyanite-rich metapelitic rocks in the aureole of the 199.1 ± 6.8 Ma Walhalla pluton (Fig. 2)
549 formed at 195.0 ± 1.7 Ma (monazite) and have an estimated pressure of 5.4-7.6 kbar at 600°C
550 (Berman et al., 2007), which is consistent with the Al-in-hornblende pressure estimate of 5.9 ±
551 0.9 kbar for the granodiorite in the pluton (Fig. 10a). North of Carmacks, Upper Triassic rocks of
552 Stikinia are locally metamorphosed to greenschist and lower amphibolite facies (Read et al.,
553 1991; Colpron et al., 2003; Colpron & Ryan, 2010).

554 Exhumation of the Minto suite plutons and their Yukon-Tanana host rocks followed
555 shortly after intrusion and peak metamorphism (Clark, 2017), and ca. 200-180 Ma mica dates
556 suggest cooling below 300-350°C in the Early Jurassic (Fig. 10b). The Minto and Granite
557 Mountain plutons were emplaced at ~20 km at ca. 198-195 Ma and exhumed by ≤10 km in 8-14
558 Myr, for average exhumation rates of 0.7-1.3 mm/yr (Sack et al., 2020). To the east, the Tatchun
559 batholith was emplaced deeper (~25 km) and exhumed ~15 km in only 2-7 Myr, for average
560 exhumation rates of 2.1-7.5 mm/yr. The higher exhumation rates suggest that unroofing may
561 have been aided by tectonic denudation. The Willow Lake fault is a low-angle extension fault
562 that is inferred to have accommodated part of the tectonic denudation in the Early Jurassic (Figs.
563 2 and 3; Colpron & Ryan, 2010). Its hanging wall contains relatively undeformed and
564 unmetamorphosed Mississippian volcanic and plutonic rocks of the Yukon-Tanana terrane that
565 preserve Mississippian mica cooling ages (Knight et al., 2013; Joyce et al., 2015). These rocks
566 formed an upper crustal lid beneath which strongly foliated, locally protomylonitic, amphibolite
567 facies metasedimentary and metaplutonic rocks in the footwall were exhumed in the Early
568 Jurassic (ca. 189-185 Ma mica cooling ages; Fig. 10b).

569 Plutons of the Long Lake (ca. 188-183 Ma) and Bennett suites (ca. 178-175 Ma) were
570 emplaced at shallower crustal levels during this Early Jurassic phase of exhumation (Figs. 8 and
571 10a). Plutons of the Long Lake suite generally yield Al-in-hornblende pressures of 3.4-5.3 kbar
572 (emplacement depths of 13-20 km) and cooled rapidly within 2-4 Myr after crystallization.
573 Similar Al-in-hornblende pressures of 4.3-5.5 kbar are reported from Early Jurassic plutons of
574 the Long Lake and Bennett suites in northern British Columbia (Currie, 1994).

575 4.2.2 *East of the BSTF*

576 The Lokken suite (ca. 195-184 Ma) intrudes the Yukon-Tanana terrane east of the BSTF.
577 It comprises mainly small plutons in Yukon but includes the large, composite Coconino–
578 Simpson Peak–Nome Lake batholith in northern British Columbia (Figs. 2, 3 and 4). Unlike the
579 Early Jurassic plutons to the west, there is no apparent pattern of age distribution in the Lokken
580 suite. The Lokken plutons are generally more mafic, locally ultramafic, metaluminous, and high-
581 K calc-alkaline to shoshonitic with subchondritic εNd_t, $^{87}Sr/^{86}Sr_i$ generally >0.7047, and εHf_t in
582 zircon of -2.9 to +9.3 (Figs. 6 and 7). Overall, the Lokken suite has a range of isotopic values
583 comparable to Minto suite plutons to the west. In contrast to Early Jurassic plutons west of the
584 BSTF, the Lokken suite shows an apparent trend of decreasing crustal influence through time,
585 with a generally more juvenile isotopic signature in younger plutons (Fig. 6). Zircon inheritance
586 is less common in Lokken suite plutons, with inherited cores encountered in only 3 of 8 samples
587 analyzed, and in younger plutons of the suite (ca. 186-184 Ma; Figs. 3 and 9). Limited Al-in-
588 hornblende data suggest emplacement depths ≤10 km (Figs. 8 and 10a), consistent with
589 predominantly greenschist facies assemblages in the Yukon-Tanana host rocks (Read et al.,
590 1991). Mica dates also suggest relatively rapid cooling within ≤2 Myr (Fig. 10b). Local

591 development of foliation and myrmekitic textures suggest emplacement during deformation and
592 metamorphism.

593 Lokken suite plutons in Yukon are probably along-strike equivalents of syn-tectonic,
594 Alaskan-type intrusions in Quesnellia and Yukon-Tanana terranes in British Columbia, including
595 the Turnagain (Fig. 3; ca. 190-185 Ma; Nixon et al., 2020) and Polaris complexes (ca. 186 Ma;
596 Nixon et al., 1997). Like the Turnagain complex, plutons of the Lokken suite locally include
597 mafic to ultramafic phases and were apparently emplaced during regional deformation and
598 metamorphism related with imbrication of Yukon-Tanana and Quesnellia with the western North
599 American margin.

600 4.3 Middle to Late Jurassic post-collisional magmatism

601 Middle Jurassic plutons of the Bryde and Fourth of July suites intruded the axis of the
602 Intermontane terranes and the overlapping Whitehorse trough (Figs. 2 and 3) after initial
603 imbrication with Stikinia and Cache Creek terranes (Mihalynuk et al., 2004; Bickerton et al.,
604 2020). The post-collisional Bryde suite is generally more alkalic with juvenile $^{87}Sr/^{86}Sr_i$
605 (<0.7047), and superchronditic εNd_t and zircon εHf_t values (Fig. 6) that indicate renewed mantle
606 input in the Middle Jurassic (ca. 174 Ma). By the Late Jurassic, peraluminous granodiorite and
607 granite of the McGregor pluton (ca. 163-146 Ma) show another shift to more evolved isotopic
608 signatures and increasing crustal input. The shift in isotopic values between the Middle and Late
609 Jurassic is similar to the trend observed in Late Triassic to Early Jurassic plutons west of the
610 BSTF (Fig. 6) and likely reflects continued crustal thickening and growth of the orogen.

4.4 Whitehorse trough

Crustal thickening and emplacement of Early Jurassic plutons were coincident with development of the Whitehorse trough (Colpron et al., 2015), a marine synorogenic sedimentary basin that overlaps Stikinia and Cache Creek terranes north of the Stikine arch (Figs. 1 and 11). Its siliciclastic fill, the Laberge Group, comprises proximal, shallow marine sandstone and conglomerate along the northern (Tanglefoot formation) and western margins (Takwahoni Formation), and generally more distal, deep-water sandstone-mudstone (turbidite) and mass-flow conglomerate of the Richthofen and Inklin formations near the centre of the basin (Wheeler, 1961; Souther, 1971; Hart, 1997; Johannson et al., 1997; English et al., 2005; Lowey, 2008). Subsidence in the Whitehorse trough began in late Hettangian to Sinemurian (ca. 199 Ma) during emplacement of the Minto suite within a thickening orogen and continued through Early Jurassic exhumation until the Bajocian (Middle Jurassic). Pliensbachian (ca. 188-186 Ma) crystal-lithic tuff of the Nordenskiöld facies occur at various stratigraphic levels within the Tanglefoot and Richthofen formations in Yukon and likely represent pyroclastic deposits sourced from magma of the Long Lake suite to the west (Colpron & Friedman, 2008). Conglomerate clasts in the Laberge Group indicate progressive unroofing of Stikinia with mostly volcanic and sedimentary clasts in Sinemurian to lower Pliensbachian strata, mostly plutonic clasts in the upper Pliensbachian, and appearance of metamorphic clasts in upper Toarcian strata (Dickie & Hein, 1995; Hart et al., 1995; Johannson et al., 1997; Shirmohammad et al., 2011). Eclogite clasts occur locally in Pliensbachian-Toarcian strata of the Laberge Group in northern British Columbia (Fig. 11; Canil et al., 2006). They record rapid exhumation in the Early Jurassic (Kellett et al., 2018). Chert clasts are locally present in Bajocian strata in Yukon (Colpron et al.,

2015) and are abundant in strata of this age in northern British Columbia (Shirmohammad et al., 2011).

Detrital zircon provenance studies show that Laberge Group rocks were locally derived from basement sources on the flanks of Whitehorse trough (Colpron et al., 2015; van Drecht, 2019). Late Triassic–Early Jurassic zircons make the dominant age peaks in Laberge sandstones with Paleozoic (mainly Carboniferous) zircons representing subordinate but locally significant populations. This pattern matches igneous ages from plutons surrounding the Whitehorse trough (Colpron et al., 2015) and inherited zircons in Jurassic plutons (Figs. 3, 4 and 9). The Hf isotopic signatures of detrital zircons in sandstones of the Laberge Group show a shift from superchondritic to subchondritic values between Late Triassic and Early Jurassic (van Drecht, 2019), a pattern that mimics the trend observed in Late Triassic and Jurassic plutons in Yukon (Fig. 6c).

Final imbrication of the Intermontane terranes in Middle Jurassic (Aalenian-Bajocian) brought the end of marine deposition in the Whitehorse trough, local tilting of Laberge strata, surface uplift and deposition of the overlying Upper Jurassic to Lower Cretaceous Tantalus Formation in fluvial and lacustrine settings within confined intermontane valleys (Long, 2015). Detrital zircons in the Tantalus Formation have mainly similar sources as, or were recycled from Laberge Group strata, with exception of minor Late Jurassic populations that Colpron et al. (2015) attributed to ash-fall from distal volcanic sources in the Insular terranes. New CA-TIMS dates from the main phase of the McGregor batholith (163-161 Ma; Fig. 4) and a $^{40}Ar/^{39}Ar$ muscovite age of ca. 146 Ma from its younger phase (Sack et al., 2020) indicate that local sources are available for Late Jurassic zircons in the Tantalus Formation.

5 Discussion

5.1 Improved geochronology and tempos of magmatism

The new zircon CA-TIMS U-Pb dates produced for this study provide tight constraints on the duration of pluton emplacement in southern Yukon (Fig. 4). These data indicate that Late Triassic to Early Jurassic suites that intrude Stikinia and Yukon-Tanana terrane west of the BSTF were emplaced in discrete episodes of 2-5 Myr in duration, possibly as long as 8-9 Myr for the Minto suite. These new data bring refinement over the apparent continuum in magmatism from Late Triassic to Middle Jurassic suggested when all U-Pb zircon dates acquired from these plutons are considered, including ages determined using less precise analytical techniques such as LA-ICPMS, secondary ion mass spectrometry (SIMS), and TIMS on multi-grain, air-abraded zircon fractions (Fig. 12). The large batholiths of the Minto suite were primarily constructed over ~3.5 Myr between 198.22 and 194.71 Ma (Figs. 4 and 12). Older, ca. 205-203 Ma phases are locally documented and the common occurrence of ca. 205-203 Ma zircon antecrysts suggest that Minto magmatism may have lasted up to 8-9 Myr. Construction of the Aishihik batholith (Long Lake suite; Fig. 3) occurred over ~3 Myr between 186.22 and 183.28 Ma, and the full range of Long Lake magmatism lasted ~4.6 Myr, from 187.46 to 182.83 Ma (Figs. 4 and 12). The Lokken suite, east of the BSTF, spans 9 Myr and includes a magmatic pulse at ca. 192 Ma during an apparent lull between the Minto and Long Lake suites to the west (Figs. 4 and 12). The tempos of magmatism indicated from the range of CA-TIMS dates in Early Jurassic plutons in Yukon are consistent with construction rates of ≤10 Myr determined for other well-studied large batholiths (e.g., Coleman et al., 2004; Glazner et al., 2004; Frazer et al., 2014; Schwartz et al., 2017).

677 Limited CA-TIMS data for the Bennett suite precludes exact estimate of the intrusive rate
678 for these plutons, however when considering previous TIMS dates a tempo of ~3 Myr is also
679 indicated. Plutons of the Middle Jurassic Bryde suite were mostly intruded in <2 Myr, between
680 173.44 and 172.62 Ma (Figs. 4 and 12). The 168.09 Ma Michie pluton could represent
681 continuum of Bryde suite magmatism over ~5.4 Myr or a distinct, younger pulse of magmatism.
682 In northern British Columbia, Mihalynuk et al. (2004, 2018) estimated a range of ca. 172-166
683 Ma for the Fourth of July suite based on U-Pb zircon TIMS, and K-Ar and $^{40}Ar/^{39}Ar$ biotite
684 dates.

685 5.2 Sources of inheritance

686 Inherited zircon cores were documented in 15 of 30 Jurassic samples analyzed both by
687 LA-ICPMS and CA-TIMS (Figs. 3 and 9). A total of 129 cores were analyzed with 54% yielding
688 Triassic to Jurassic (ca. 235-187 Ma), 37% Devonian to Carboniferous (ca. 378-306 Ma), 4%
689 Permian (ca. 275-250 Ma), and 5% Precambrian dates (ca. 2606-571 Ma; Fig. 9e). Late Triassic
690 cores (peak at 213 Ma) are most common in the Minto suite, although Paleozoic cores make up
691 the majority of zircon xenocrysts analyzed in these samples (68%; Fig. 9a). The Late Triassic
692 zircon cores have juvenile εHf_t values (+3.2 to +6.0), similar to those of the Stikine–Lewes River
693 arc (whole rock εHf_t +3.2 to +10.6; Fig. 9f); this is consistent with the local abundance of
694 variably migmatized xenoliths of Late Triassic intermediate to mafic rocks in plutons of the
695 Minto suite (Kovacs et al., 2020; Sack et al., 2020).
696 Inherited zircons in samples of the Long Lake, Lokken and McGregor suites are
697 dominated by latest Triassic to Early Jurassic dates (ca. 209-193 Ma) with ca. 199 Ma peaks and
698 εHf_t values of -6.0 to +9.3 (Fig. 9). These peaks match well with the age range of the Minto suite
699 (Fig. 4), but igneous zircons from these plutons are consistently superchondritic (εHf_t +0.5 to

700 +10.9; Fig. 6). Occurrences of Minto-age xenocrysts in Early Jurassic granitoids from both sides
701 of the BSTF point to similarity in latest Triassic to earliest Jurassic magmatic activity, although
702 plutons older than ca. 195 Ma are not documented in the Lokken suite in Yukon. The oldest
703 phases in the Hogem batholith of central British Columbia (Fig. 1) are ca. 207-194 Ma (Jones et
704 al., 2021) and older plutons (ca. 215-205 Ma) are common in southern Quesnellia (Mortensen et
705 al., 1995; Han et al., 2020).

706 Inherited zircons with Paleozoic dates are present in all suites and generally match well
707 the ages and Hf isotopic composition of local Paleozoic units in Yukon-Tanana and Stikinia (Fig.
708 9f). The Late Devonian inherited zircons (ca. 378-374 Ma) with mostly subchondritic εHf_t values
709 in the Aishihik batholith (Long Lake suite) are the exception (Fig. 9). There are no known
710 sources in local rocks of Stikinia or Yukon-Tanana terrane for these zircons. In southern Yukon,
711 ca. 378-373 Ma volcanism is only documented in continental margin strata of the Earn Group,
712 presently ~250 km away northeast of the Tintina fault (Yukon Geological Survey, 2020c;
713 Cobbett et al., 2021). Zircons within this age range are also documented in the Yukon-Tanana
714 terrane of southeast Alaska (>400 km south) but consistently have superchondritic εHf_t values
715 (Pecha et al., 2016). Rare Precambrian zircons in Early Jurassic plutons in Yukon were likely
716 recycled through incorporation of minor metasedimentary sources in the Yukon-Tanana terrane
717 (e.g., Snowcap assemblage; Piercey & Colpron, 2009).

718 5.3 Spatial vs. temporal isotopic patterns

719 Armstrong (1988) showed that the regional distribution of $^{87}Sr/^{86}Sr_i$ isopleths in
720 Mesozoic igneous rocks of the Canadian Cordillera defines a hairpin geometry with juvenile
721 values ($\leq$0.704) in the core of the Intermontane terranes surrounded by more evolved values
722 ($\geq$0.705) in central Yukon. This pattern was one of the lines of evidence that led to the oroclinal

723 entrapment model of Mihalynuk et al. (1994). The new isotopic data reported here confirm the
724 general patterns of $^{87}Sr/^{86}Sr_i$ isopleths (Fig. 7a) observed by Armstrong (1988) but with the
725 added benefit of improved geochronological constraints (Fig. 4). As noted above, the isotopic
726 evolution of Late Triassic and Jurassic plutons in southern Yukon is directly linked with the age
727 of magmatism, with Early Jurassic plutons west of the BSTF yielding more evolved values in
728 progressively younger plutons, and those east of the BSTF showing a reverse trend (Fig. 6).
729 Juvenile isotopic values are mainly documented in plutons of the Late Triassic Stikine suite and
730 Middle Jurassic Bryde suite that only occur southwest of the BSTF (Fig. 7). Juvenile $^{87}Sr/^{86}Sr_i$
731 (<0.704) values are only documented in one pluton of the Lokken suite, east of the BSTF, and
732 the distribution of isopleths is likely somewhat modified by Cretaceous or younger displacement
733 along the fault zone.

734 5.4 Redefining terrane boundaries

735 The difference in style of Early Jurassic magmatism across the BSTF provides new
736 constraints on locating the boundary between Stikinia and Quesnellia in central Yukon (Figs. 3
737 and 11). In British Columbia, the two arc terranes occur on either side of the Cache Creek
738 accretionary complex, but in Yukon the absence of Cache Creek rocks north of ~61°N have
739 made the distinction between Stikinia and Quesnellia difficult (Fig. 1). The Thibert fault marks
740 the boundary between Quesnellia and Cache Creek terranes in northern British Columbia and its
741 extension in Yukon, the Teslin fault, has traditionally been inferred to mark the Quesnellia-
742 Stikinia boundary (Gordey & Makepeace, 2001; Colpron, 2011; White et al., 2012; Colpron et
743 al., 2016b). Near 62°N in central Yukon, seismic and gravity results suggest that the Big Salmon
744 fault is a more significant crustal structure than the Teslin fault (Calvert et al., 2017).

745 The peraluminous plutons of the Minto suite that were emplaced at lower crustal levels
746 are restricted to the west of the BSTF (Figs. 2 and 3). East of Carmacks, the Tatchun batholith
747 intrudes Carboniferous rocks of the Boswell assemblage and overlying Upper Triassic volcanic
748 rocks of the Semenof formation (Tempelman-Kluit, 1984, 2009; Colpron, 2011). Augite-phyric
749 volcanic and volcaniclastic rocks and minor Carnian-Norian limestone of the Semenof formation
750 resemble coeval strata of the Lewes River Group to the west (Fig. 2). They unconformably
751 overlie mafic to intermediate metavolcanic, metavolcaniclastic and metasedimentary rocks
752 (Boswell assemblage) which have been interpreted to represent local Paleozoic basement to
753 Quesnellia (Colpron, 2011). Their association with Minto suite plutons suggests, however, that
754 they are part of the same crustal panel as Stikinia west of the Teslin fault.
755 East of the BSTF, metaluminous plutons of the Lokken suite were emplaced at higher
756 crustal levels into part of the Yukon-Tanana terrane that includes strata of the Klinkit
757 assemblage, which are correlated with Paleozoic arc successions of Quesnellia in British
758 Columbia (Lay Range assemblage; Ferri, 1997; Simard et al., 2003; Nelson & Friedman, 2004;
759 Roots et al., 2006; Nixon et al., 2020). The Lokken suite is generally more mafic than Early
760 Jurassic plutons west of the BSTF and locally includes ultramafic phases (Roots et al., 2004).
761 Upper Triassic rocks overlying Yukon-Tanana east of the BSTF are fine-grained siliciclastic
762 rocks and local conglomerate that are inferred to correlate with those overlapping the western
763 Laurentian margin (Unterschutz et al., 2002; Colpron et al., 2006a; Beranek & Mortensen, 2011;
764 Golding et al., 2016).
765 The present crustal architecture of the Intermontane terranes in central Yukon was
766 acquired through superposition of Jurassic to Late Cretaceous (and younger) structures (Nelson
767 et al., 2013; Calvert et al., 2017). The Cretaceous structures dissected and overprinted older

Jurassic faults such as the Tadru and Needlerock faults (Figs. 2 and 3; Colpron et al., 2002, 2003). The Needlerock thrust is a folded thrust fault that juxtaposes the Snowcap assemblage (Yukon-Tanana terrane) in its hanging wall with greenstone and amphibolite of the Boswell assemblage in its footwall. The Boswell assemblage was intruded at mid to lower crustal level by the Tatchun batholith (Minto suite) in the Early Jurassic, suggesting that the Needlerock thrust may be a remnant of the Jurassic boundary between Stikinia to the west and Yukon-Tanana/Quesnellia to the east. Extension of the Needlerock thrust, and the Stikinia-Quesnellia boundary, into western Yukon remains enigmatic.

5.5 Relationship to Hazelton arc

The syn-collisional intrusion of Early Jurassic plutons and development of the Whitehorse trough north of the Stikine arch contrasts with continued Early to Middle Jurassic arc activity recorded in volcano-sedimentary strata of the Hazelton Group to the south (Fig. 11; Gagnon et al., 2012; Nelson et al., 2018, 2022; George et al., 2021). Widespread exposures of the Hazelton Group across 300 km in northern British Columbia, between the Stikine and Skeena arches, were interpreted by Marsden and Thorkelson (1992) to result from development of two magmatic arcs above opposing subduction zones on either side of Stikinia. However, more recent studies show that Rhaetian to Toarcian arc magmatism in the lower Hazelton Group focussed on an arcuate belt that spans the Skeena arch (including the Telkwa and Toodoggone formations) and that coeval magmatism in the Stewart-Iskut region formed in the back-arc (Fig. 11; Nelson et al., 2018, 2022; George et al., 2021). The onset of lower Hazelton arc magmatism (ca. 205-200 Ma) coincides with initial collision and intrusion of the Minto suite north of the Stikine arch. Following initial collision, the Hazelton arc is inferred to have migrated southward through the Early Jurassic. Subduction rollback was accommodated by north-south extension and

subsidence in the back-arc region (e.g., Diakow et al., 1993; Diakow & Rhodes, 2006; Gagnon et al., 2009; Nelson et al., 2022). Sinistral transpression along structures such as the Llewellyn and Wann River faults (Currie & Parrish, 1993; Mihalynuk et al., 1999) probably linked the retreating Hazelton arc with the collision zone, Early Jurassic extensional exhumation of the Yukon-Tanana terrane, and subsidence of the Whitehorse trough north of the Stikine arch (Fig. 11). Early Jurassic syn-collisional plutons in Stikinia north of the Stikine arch show a southward migration that suggests that the source of magmatism remained tied to the supra-subduction mantle wedge associated with the retreating Hazelton arc.

South of the Stikine arch, post-arc extension and subsidence is recorded by predominantly sedimentary strata of the upper Hazelton Group (Pliensbachian-Callovian), which onlapped the arch in Toarcian, and development of the Eskay rift in Aalenian-Bajocian (Gagnon et al., 2012; Barresi et al., 2015; Nelson et al., 2018). The Hazelton Group is conformably overlain by southward-propagating synorogenic clastic rocks of the Middle Jurassic to Lower Cretaceous Bowser Lake Group (Evenchick et al., 2007, 2010).

Detrital zircons in sandstones from the Hazelton Group are dominated by Triassic and Jurassic ages that resemble age distribution in strata of the Laberge Group in Yukon (Colpron et al., 2015; George et al., 2021). However, Triassic-Jurassic zircons in the Hazelton Group in central Stikinia have consistently juvenile εHf_t values (George et al., 2021) that contrast with the isotopic pull-down observed in detrital zircons from the Laberge Group (van Drecht, 2019) and in igneous zircons from Early Jurassic syn-collisional plutons of southern Yukon (Fig. 6c).

5.6 Tectonic evolution

Over the last 25 years, the oroclinal entrapment of the Cache Creek terrane has been the prevalent tectonic model for the Jurassic evolution of the Intermontane terranes in the Canadian

814 Cordillera (Nelson & Mihalynuk, 1993; Mihalynuk et al., 1994, 2004; Nelson et al., 2013;
815 Colpron et al., 2015). In this model, similar late Paleozoic–early Mesozoic arc terranes of
816 Stikinia and Quesnellia, which include Permian and Triassic fauna endemic to southern
817 Laurentia (Stevens, 1995; Stanley & Senowbari-Daryan, 1999; Belasky et al., 2002), were
818 oroclinally folded around the accretionary complex of the Cache Creek terrane containing
819 Permian faunal elements of Tethyan (exotic) affinity (Ross & Monger, 1978; Ross & Ross,
820 1983). Oroclinal enclosure was thought to be triggered by introduction of oceanic plateaus
821 (Mihalynuk et al., 1994) or primitive arc crust (Kutcho assemblage; Colpron et al., 2015) into the
822 Late Triassic subduction zone, and the axial region of the Stuhini-Lewes River arc rotated
823 counterclockwise around a hinge zone in the Yukon-Tanana terrane relative to the arc axis of
824 Quesnellia. A challenge with this model is the implied ≥90° rotation, around a vertical axis, of a
825 subduction zone with slab width ≥2000 km that would have been characterized by a southward
826 increase in retreat velocities of the trench, possibly exceeding 12 cm/yr near the south end of
827 Stikinia (assuming angular rotation of as much as 2500 km in ~20 Myr). Modelling of modern
828 subduction zones, however, shows that for slabs ≥2000 km trench retreat velocities are slow (to
829 nearly stationary) near the centre of the slab, generally ≤2 cm/yr (Schellart et al., 2007). Faster
830 velocities (up to 6-16 cm/yr) are only observed in narrow slabs (≤1500 km) with curved, convex
831 geometries, such as the Oligocene to Holocene Scotia and Calabrian subduction zones.
832 Additionally, three-dimensional numerical modelling of continental ribbons with horizontally
833 stratified lithosphere (as observed in arc crust; Calvert, 2011) show that horizontal-axis folding
834 and thickening of the lithosphere is more probable than vertical-axis rotation of an orocline
835 (Smith et al., 2021). Thus, it is improbable that the Stikinia subduction zone was subject of
836 wholesale angular rotation in the Early Jurassic, as implied in some recent models (Logan &

837 Mihalynuk, 2014; Colpron et al., 2015). Alternative models invoking strike-slip duplication of
838 the Quesnellia-Stikinia arc have been proposed (Wernicke & Klepacki, 1988), but fail to explain
839 the concentric south-facing patterns of geological elements in the northern Intermontane terranes
840 (Figs. 1 and 2). Detailed documentation of the Early Jurassic collision zone north of the Stikine
841 arch provides new constraints and the basis for an alternative model (Fig. 13).

842 The configuration of Triassic arc terranes outboard of western Laurentia is inferred to
843 have resembled a mirror image of the present-day geometry of the western Aleutian and
844 Kamchatka subduction zones, where parts of Quesnellia (and its Yukon-Tanana basement in the
845 north) were anchored on the margin of western Pangea (Unterschutz et al., 2002; Beranek &
846 Mortensen, 2011) and Stikinia extended westward into an intra-oceanic island arc festoon (Fig.
847 13a; Mihalynuk et al., 1994; Colpron et al., 2015; George et al., 2021). Plutons of the Stikine and
848 Pyroxene Mountain suites in Yukon indicate that Stikinia was locally anchored on the Yukon-
849 Tanana terrane by the Late Triassic. Other parts of the Late Triassic Stikinia arc (present-day
850 northern and central British Columbia) appear to have been constructed on distinct Paleozoic
851 basement with probable affinity to the Insular terranes (George et al., 2021). Late Triassic
852 (Carnian-Norian) volcanic and sedimentary rocks of Stikinia also unconformably overlie Middle
853 Triassic volcanic units that form part of the Kutcho assemblage in southern Yukon and northern
854 British Columbia and indicate juxtaposition prior to development of the Stikine arc (e.g., Logan
855 et al., 2012; Schiarizza, 2012; Bordet et al., 2019). This postulated arc configuration suggests
856 that plate motion in Panthalassa was northeasterly in the Late Triassic.

857 End-on arc collision in northern Stikinia was likely triggered by onset of the
858 northwestward drift of North America as break-up of the Pangea supercontinent began in latest
859 Triassic (Coney, 1972; Dickinson, 2004; Monger & Gibson, 2019). This resulted in initial

imbrication and crustal thickening of the northern Intermontane terranes, north of the Stikine arch, and intrusion of Minto suite plutons that are transitional between arc and syn-collisional granitoids and show increased crustal influence (Figs. 6 and 13b). Subduction waned beneath the Stuhini-Lewes River arc north of the Stikine arch and part of the slab was reconfigured into a shorter segment above which the Hazelton arc was developed to the south (Nelson et al., 2022). The Sinemurian exhumation of eclogite bodies, recorded as clasts in Pliensbachian strata of the Laberge Group (Kellett et al., 2018), may have been facilitated by slab tear associated with this subduction reconfiguration. To the east, subduction of Panthalassa lithosphere continued beneath Quesnellia (Fig. 13b).

Between Sinemurian and Toarcian, the Hazelton trench retreated to the south and back-arc extension occurred south of the Stikine arch (Fig. 13c; Nelson et al., 2022). This evolving arc–back-arc system was probably linked to the collision zone to the north by sinistral strike-slip faults such as the Llewelyn fault (Fig. 11). Sinistral transtension likely accommodated extensional exhumation of the burgeoning orogen and subsidence of the Whitehorse trough to the north (van Drecht, 2019). Subsidence may have been aided by underplating of mafic crust and development of an eclogitic root after cessation of Late Triassic subduction. Isotopically evolved granitoid plutons of the Long Lake and Bennett suites were emplaced within the exhuming orogen. In this revised model, entrapment of the Cache Creek terrane occurred as a result of development of sinistral transform faults that were linked to the retreating Hazelton subduction zone.

Continued westward drift of North America, as opening of the central Atlantic Ocean began, possibly as early as late Sinemurian (Labails et al., 2010), resulted in convergence of the Intermontane terranes with the North American continental margin in late Sinemurian to

Pliensbachian (Murphy et al., 1995; Nixon et al., 1997, 2020). Paleomagnetic data and faunal assemblages from strata in Stikinia suggest it was approximately 11.2 ± 6.1° (1200 ± 680 km) south of its present position relative to the North American craton in late Sinemurian to early Pliensbachian (Smith et al., 2001; Smith, 2006; Kent & Irving, 2010). The collision zone now located in southern Yukon was then probably at similar latitude as present-day southern Aberta, and the easterward convergence of the accreted terranes likely drove the onset of subsidence and deposition of the Fernie Formation in the Alberta foreland basin (Fig. 13c; Cant & Stockmal, 1989; Asgar-Deen, 2003; McCartney, 2012; Colpron et al., 2015; Pană et al., 2018).

By Middle Jurassic, subduction had ceased beneath Quesnellia, blueschists were exhumed in the northern Cache Creek terrane, and the Intermontane terranes were imbricated along a series of west-verging thrust faults (Fig. 13d; Mihalynuk et al., 2004). The post-collisional plutons of the Bryde suite are characterized by a return to isotopically juvenile magmatism at ca. 174 Ma (Fig. 6) that suggests asthenospheric upwelling following terrane imbrication. This coincides with surface uplift that marked the end of marine deposition in Whitehorse trough and development of intermontane river systems recorded in strata of the Tantalus Formation. The combination of juvenile magmatism and surface uplift suggests that lithospheric delamination or slab breakoff occurred following final collision of the northern Intermontane terranes (e.g., Kay & Kay, 1993; Davies & von Blanckenburg, 1995; von Blanckenburg & Davies, 1995).

6 Conclusions

The Late Triassic to Jurassic plutons in the Intermontane terranes of Yukon record the transition from arc to syn- and post-collisional magmatism. Juvenile Late Triassic magmatism of the Stikine and Pyroxene Mountain suites represent the northern extension of the Stikinia arc that

906 locally intrudes the Yukon-Tanana terrane in Yukon and Alaska. The Early Jurassic plutons west
907 of the BSTF in Yukon were intruded into a thickening orogen and show increasing crustal
908 contributions with time. This contrasts with coeval, juvenile magmatism of the Hazelton arc in
909 British Columbia that apparently records a southward arc migration in the Early Jurassic. East of
910 the BSTF, Early Jurassic plutons that intrude into Yukon-Tanana basement are the northern
911 extension of Quesnellia arc magmatism. Syn-collisional, Early Jurassic magmatism in Yukon is
912 interpreted to result from end-on arc collision in northern Stikinia. Exhumation of the Yukon-
913 Tanana terrane and coeval subsidence in the Whitehorse trough developed as a result of sinistral
914 transtension linked to the retreating Hazelton trench to the south. A revised tectonic model shows
915 that entrapment of the Cache Creek terrane is the result of Hazelton slab rollback and
916 development of sinistral transform faults that originated from the collision zone to the north. The
917 continued westward drift of the North American continent resulted in imbrication and final
918 accretion of the Intermontane terranes in the Middle Jurassic. This was accompanied by
919 lithospheric delamination as indicated by a return to juvenile magmatism in Middle Jurassic and
920 surface uplift that marked the end of marine deposition in the Whitehorse trough.

921 **Acknowledgments**

922 Discussions with JoAnne Nelson, Sarah George and Bram van Straaten provided insights
923 in developing the alternative model proposed in this paper. Comments by Bill McClelland, Jim
924 Monger, Don Murphy and JoAnne Nelson on early versions of the manuscript have helped
925 sharpen the arguments. Formal reviews by Mitch Mihalynuk and an anonymous reviewer, and
926 editorial advices by Associate Editor Robinson Cecil are gratefully acknowledged. This study
927 was funded by the Yukon Geological Survey with additional support by Natural Resources

Canada's Geomapping for Energy and Minerals program. This is Yukon Geological Survey contribution #058.

Data Availability

Data for this paper are available for download from:

1) Sack, P.J., Colpron, M., Crowley, J.L., Ryan, J.J., Allan, M.M., Beranek, L.P., Joyce, N.L., Mortensen, J.K., Israel, S. & Chapman, J.B. (2020). Atlas of Late Triassic to Jurassic plutons in the Intermontane terranes of Yukon [Dataset]. Yukon Geological Survey, Open File 2020-1, 365 p., 13 digital appendices, http://data.geology.gov.yk.ca/Reference/95839.
2) Sack, P.J., Colpron, M. & Crowley, J.L. (2022). U-Pb zircon geochronology from a Late Triassic pluton in the Mount Nansen area [Dataset]. Yukon Geological Survey, Open File 2022-2, 7 p., 2 digital appendices, https://data.geology.gov.yk.ca/Reference/95925.

References

Anderson, J. L., & Smith, D. R. (1995). The effects of temperature and fO_2 on the Al-in-hornblende barometer, *American Mineralogist, 80*, 549-559.

Armstrong, R. L. (1988). Mesozoic and early Cenozoic magmatic evolution of the Canadian Cordillera, In Clark, S. P., Jr., Burchfield, B. C., & Suppe, J. (Eds.), *Processes in Continental Lithospheric Deformation*, *Special Paper* (218, pp. 55-91). Boulder, CO: Geological Society of America.

Asgar-Deen, M. (2003). *Stratigraphy, sedimentology and paleogeography of the Lower Jurassic Nordegg Member (Gordondale Member), west-central Alberta* (M.Sc. thesis). University of Calgary.

950 Barresi, T., Nelson, J. L., Dostal, J., & Friedman, R. M. (2015). Evolution of the Hazelton arc near
951 Terrace, British Columbia: Stratigraphic, geochronological, and geochemical constraints on a
952 Late Triassic-Early Jurassic arc and Cu-Au porphyry belt, *Canadian Journal of Earth Sciences,*
953 *52*, 466-494.
954 Beatty, T. W., Orchard, M. J., & Mustard, P. S. (2006). Geology and tectonic history of the Quesnel
955 terrane in the area of Kamloops, British Columbia, In Colpron, M., & Nelson, J. L. (Eds.),
956 *Paleozoic Evolution and Metallogeny of Pericratonic Terranes at the Ancient Pacific Margin of*
957 *North America*, *Special Paper* (45, pp. 483-504). St. John's, NL: Geological Association of
958 Canada.
959 Belasky, P., Stevens, C. H., & Hanger, R. A. (2002). Early Permian location of western North American
960 terranes based on brachiopod, fusulinid and coral biogeography, *Palaeogeography,*
961 *Palaeoclimatology, Palaeoecology, 179*, 245-266.
962 Beranek, L. P., & Mortensen, J. K. (2011). The timing and provenance record of the Late Permian
963 Klondike orogeny in northwestern Canada and arc-continent collision along western North
964 America, *Tectonics, 30*, TC5017, https://10.1029/2010TC002849.
965 Berman, R. G., Ryan, J. J., Gordey, S. P., & Villeneuve, M. (2007). Permian to Cretaceous
966 polymetamorphic evolution of the Stewart River region, Yukon-Tanana terrane, Yukon, Canada:
967 P–T evolution linked with *in situ* SHRIMP monazite geochronology, *Journal of metamorphic*
968 *Geology, 25*, 803-827.
969 Bickerton, L., Colpron, M., Gibson, H. D., Thorkelson, D. J., & Crowley, J. L. (2020). The northern
970 termination of the Cache Creek terrane in Yukon: Middle Triassic arc activity and Jurassic-
971 Cretaceous structural imbrication, *Canadian Journal of Earth Sciences, 57*, 227-248,
972 https://doi.org/10.1139/cjes-2018-0216.

973 Bordet, E., Crowley, J. L., & Piercey, S. J. (2019). *Geology of eastern Lake Laberge area (105E), south-*
974 *central Yukon*. (Open File 2019-1). Whitehorse, YT: Yukon Geological Survey.
975 British Columbia Geological Survey (2019). *BC MINFILE - A database of mineral occurrences*.
976 (https://www2.gov.bc.ca/gov/content/industry/mineral-exploration-mining/british-columbia-
977 geological-survey/mineralinventory).
978 Brown, D. A., Gunning, M. H., & Greig, C. J. (1996). *The Stikine project: Geology of western*
979 *Telegraph Creek map area, northwestern British Columbia (NTS 104G/5, 6, 11W, 12 and 13)*.
980 (Bulletin 95). Victoria, B.C.: British Columbia Geological Survey.
981 Brown, D., Ryan, P. D., Afonso, J. C., Boutelier, D., Burg, J.-P., Byrne, T., Calvert, A. J., Cook, F.,
982 DeBari, S., Dewey, J. F., Gerya, T. V., Harris, R., Herrington, R., Konstantinovskaya, E.,
983 Reston, T., & Zagorevski, A. (2011). Arc–continent collision: The making of an orogen, In
984 Brown, D., & Ryan, P. D. (Eds.), *Arc–Continent Collision*. *Frontiers in Earth Sciences* (pp. 477-
985 493). Berlin Heidelberg: Springer-Verlag.
986 Calvert, A. J. (2011). The seismic structure of island arc crust, In Brown, D., & Ryan, P. D. (Eds.), *Arc-*
987 *Continent Collision*. *Frontiers in Earth Sciences* (pp. 87-119). Berlin Heidelberg: Springer-
988 Verlag.
989 Calvert, A. J., Hayward, N., Vayavur, R., & Colpron, M. (2017). Seismic and gravity constraints on the
990 crustal architecture of the Intermontane terranes, central Yukon, *Canadian Journal of Earth*
991 *Sciences, 54*, 798-811.
992 Canil, D., Mihalynuk, M. G., & Charnell, C. (2006). Sedimentary record for exhumation of ultrahigh
993 pressure (UHP) rocks in the northern Cordillera, British Columbia, Canada, *Geological Society*
994 *of America Bulletin, 118*, 1171-1184.

995 Cant, D. J., & Stockmal, G. S. (1989). The Alberta foreland basin: relationship between stratigraphy and
996 Cordilleran terrane-accretion events, *Canadian Journal of Earth Sciences, 26*, 1964-1975.
997 Cawood, P. A., Kröner, A., Collins, W. J., Kusky, T. M., Mooney, W. D., & Windley, B. F. (2009).
998 Accretionary orogens through Earth history, In Cawood, P. A., & Kröner, A. (Eds.), *Earth*
999 *Accretionary Systems in Space and Time*. *Special Publications* (318, pp. 1-36): Geological
1000 Society of London.
1001 Clark, A. D. (2017). *Tectonometamorphic history of mid-crustal rocks at Aishihik Lake, southwest*
1002 *Yukon* (M.Sc. thesis). Simon Fraser University.
1003 Cobbett, R., Colpron, M., Crowley, J. L., Cordey, F., Blodgett, R. B., & Orchard, M. J. (2021). Late
1004 Devonian magmatism and clastic deposition in the upper Earn Group (central Yukon) mark the
1005 transition from passive to active margin along western Laurentia, *Canadian Journal of Earth*
1006 *Sciences, 58*, 471-494, https://10.1139/cjes-2020-0161.
1007 Coleman, D. S., Gray, W., & Glazner, A. F. (2004). Rethinking the emplacement and evolution of zoned
1008 plutons: Geochronologic evidence for incremental assembly of the Tuolumne Intrusive Suite,
1009 California, *Geology, 32*, 433-436.
1010 Colpron, M. (2011). *Geological compilation of Whitehorse trough - Whitehorse (105D), Lake Laberge*
1011 *(105E), and part of Carmacks (115I), Glenlyon (105L), Aishihik Lake (115H), Quiet Lake (105F)*
1012 *and Teslin (105C)* (Geoscience Map 2011-1). Whitehorse, YT: Yukon Geological Survey.
1013 Colpron, M., & Friedman, R. M. (2008). U-Pb zircon ages for the Nordenskiold formation (Laberge
1014 Group) and Cretaceous intrusive rocks, Whitehorse trough, Yukon, In Emond, D. S., Blackburn,
1015 L. R., Hill, R. P., & Weston, L. H. (Eds.), *Yukon Exploration and Geology 2007* (pp. 139-151):
1016 Whitehorse, YT: Yukon Geological Survey.

1017 Colpron, M., & Nelson, J. L. (2009). A Palaeozoic Northwest Passage: incursion of Caledonian,
1018 Baltican and Siberian terranes into eastern Panthalassa, and the early evolution of the North
1019 American Cordillera, In Cawood, P. A., & Kröner, A. (Eds.), *Earth Accretionary Systems in*
1020 *Space and Time*. *Special Publications* (318, pp. 273-307): London, UK: Geological Society of
1021 London.
1022 Colpron, M., & Nelson, J. L. (2011). *A digital atlas of terranes for the northern Cordillera*.
1023 (http://data.geology.gov.yk.ca/Compilation/2). Whitehorse, YT: Yukon Geological Survey.
1024 Colpron, M., & Ryan, J. J. (2010). Bedrock geology of southwest McQuesten (NTS 115P) and part of
1025 northern Carmacks (NTS 115I) map area, In MacFarlane, K. E., Weston, L. H., & Blackburn, L.
1026 R. (Eds.), *Yukon Exploration and Geology 2009* (pp. 159-184). Whitehorse, YT: Yukon
1027 Geological Survey.
1028 Colpron, M., Crowley, J. L., Gehrels, G. E., Long, D. G. F., Murphy, D. C., Beranek, L. P., & Bickerton,
1029 L. (2015). Birth of the northern Cordilleran orogen, as recorded by detrital zircons in Jurassic
1030 synorogenic strata and regional exhumation in Yukon, *Lithosphere, 7*, 541-562.
1031 Colpron, M., Israel, S., & Friend, M. (2016a). *Yukon plutonic suites* (Open File 2016-37). Whitehorse,
1032 YT: Yukon Geological Survey.
1033 Colpron, M., Israel, S., Murphy, D. C., Pigage, L. C., & Moynihan, D. (2016b). *Yukon Bedrock Geology*
1034 *Map* (Open File 2016-1). Whitehorse, YT: Yukon Geological Survey.
1035 Colpron, M., Mortensen, J. K., Gehrels, G. E., & Villeneuve, M. E. (2006b). Basement complex,
1036 Carboniferous magmatism and Paleozoic deformation in Yukon-Tanana terrane of central
1037 Yukon: Field, geochemical and geochronological constraints from Glenlyon map area, In
1038 Colpron, M., & Nelson, J. L. (Eds.), *Paleozoic Evolution and Metallogeny of Pericratonic*

Terranes at the Ancient Pacific Margin of North America, Canadian and Alaskan Cordillera Special Paper (45, pp. 131-151): St. John's, NL: Geological Association of Canada.

Colpron, M., Murphy, D. C., Nelson, J. L., Roots, C. F., Gladwin, K., Gordey, S. P., Abbott, G., & Lipovsky, P. S. (2002). *Preliminary geological map of Glenlyon (105L/1-7,11-14) and northeast Carmacks (115I/9,16) areas, Yukon Territory (1:125 000 scale)* (Open File 2002-9). Whitehorse, YT: Yukon Geological Survey.

Colpron, M., Murphy, D. C., Nelson, J. L., Roots, C. F., Gladwin, K., Gordey, S. P., & Abbott, J. G. (2003). Yukon Targeted Geoscience Initiative, Part 1: Results of accelerated bedrock mapping in Glenlyon (105L/1-7,11-14) and northeast Carmacks (115I/9,16) areas, central Yukon, In Emond, D. S., & Lewis, L. L. (Eds.), *Yukon Exploration and Geology 2002* (pp. 85-108). Whitehorse, YT: Yukon Geological Survey.

Colpron, M., Nelson, J. L., & Murphy, D. C. (2006a). A tectonostratigraphic framework for the pericratonic terranes of the northern Cordillera, In Colpron, M., & Nelson, J. L. (Eds.), *Paleozoic Evolution and Metallogeny of Pericratonic Terranes at the Ancient Pacific Margin of North America, Canadian and Alaskan Cordillera Special Paper* (45, pp. 1-23): St. John's, NL: Geological Association of Canada.

Colpron, M., Nelson, J. L., & Murphy, D. C. (2007). Northern Cordilleran terranes and their interactions through time, *GSA Today, 17 (4/5)*, 4-10.

Coney, P. J. (1972). Cordilleran tectonics and North American plate motions, *American Journal of Science*, *272*, 603–628.

Coney, P. J., Jones, D. L., & Monger, J. W. H. (1980). Cordilleran suspect terranes, *Nature*, *288*, 329-333.

1061 Cook, F. A., Clowes, R. M., Snyder, D. B., van der Velden, A. J., Hall, K. W., Erdmer, P., & Evenchick,
1062 C. A. (2004). Precambrian crust beneath the Mesozoic northern Canadian Cordillera discovered
1063 by Lithoprobe seismic reflection profiling, *Tectonics*, *23*, TC2010,
1064 https://10.1029/2002TC001412.
1065 Cordey, F. (2020). Timing of Cache Creek Ocean closure: Insights from new Jurassic radiolarian ages in
1066 British Columbia and Yukon and their significance for Canadian Cordillera tectonics, *Canadian*
1067 *Journal of Earth Sciences, 57*, 1167-1179.
1068 Cordey, F., Gordey, S. P., & Orchard, M. J. (1991). New biostratigraphic data for the northern Cache
1069 Creek terrane, Teslin map area, southern Yukon, In *Current Research, Part E* (Paper 91-1E, pp.
1070 67-76). Ottawa, ON: Geological Survey of Canada.
1071 Creaser, R. A., Heaman, L. M., & Erdmer, P. (1997a). Timing of high-pressure metamorphism in the
1072 Yukon-Tanana terrane, Canadian Cordillera: constraints from U-Pb zircon dating of eclogite
1073 from the Teslin tectonic zone, *Canadian Journal of Earth Sciences, 34*, 709-715.
1074 Creaser, R. A., Goodwin-Bell, J. S., & Erdmer, P. (1999). Geochemical and Nd isotopic constraints for
1075 the origin of eclogite protoliths, northern Cordillera: implications for the Paleozoic tectonic
1076 evolution of the Yukon-Tanana terrane, *Canadian Journal of Earth Sciences, 36*, 1697-1709.
1077 Creaser, R. A., Erdmer, P., Stevens, R. A., & Grant, S. L. (1997). Tectonic affinity of Nisutlin and Anvil
1078 assemblage strata from the Teslin tectonic zone, northern Canadian Cordillera: Constraints from
1079 neodymium isotope and geochemical evidence, *Tectonics, 16*, 107-121.
1080 Cui, Y., Miller, D., Schiarizza, P., & Diakow, L. J. (2017). *British Columbia digital geology* (Open File
1081 2017-8). Victoria, BC: British Columbia Ministry of Energy, Mines and Petroleum Resources,
1082 British Columbia Geological Survey.

1083 Currie, L. D. (1994). *The geology and mid-Jurassic amalgamation of Tracy Arm terrane and Stikinia of*
1084 *northwestern British Columbia* (Ph.D. thesis). Ottawa, ON: Carleton University.
1085 Currie, L. D., & Parrish, R. R. (1993). Jurassic accretion of Nisling terrane along the western margin of
1086 Stikinia, Coast Mountains, northwestern British Columbia, *Geology, 21*, 235-238.
1087 Davies, J. H., & von Blanckenburg, F. (1995). Slab breakoff: A model of lithosphere detachment and its
1088 test in the magmatism and deformation of collisional orogens, *Earth and Planetary Science*
1089 *Letters, 129*, 85-102.
1090 Dehkordi, B. H., Ferguson, I. J., Jones, A. G., & Ledo, J. (2019). Tectonics of the northern Canadian
1091 Cordillera imaged using modern magnetotelluric analysis, *Tectonophysics, 765*, 102-128.
1092 Diakow, L. J., & Rhodes, R. (2006). Geology between the Toodoggone River and Chukachida Lake
1093 (parts of NTS 94E/6, 7, 10 and 11), north-central British Columbia, In *Geological Fieldwork*
1094 *2005* (Paper 2006-1, pp. 29-38): Victoria, BC: British Columbia Ministry of Energy, Mines and
1095 Petroleum Resources, British Columbia Geological Survey.
1096 Diakow, L. J., Panteleyev, A., & Schroeter, T. G. (1993). *Geology of the Early Jurassic Toodoggone*
1097 *Formation and gold-silver deposits in the Toodoggone River map area, northern British*
1098 *Columbia* (Bulletin 86). Victoria, BC: British Columbia Ministry of Energy, Mines and
1099 Petroleum Resources, British Columbia Geological Survey.
1100 Dickie, J. R., & Hein, F. J. (1995). Conglomeratic fan deltas and submarine fans of the Jurassic Laberge
1101 Group, Whitehorse trough, Yukon Territory, Canada - Fore-arc sedimentation and unroofing of a
1102 volcanic island-arc complex, *Sedimentary Geology, 98*, 263-292.
1103 Dostal, J., Gale, V., & Church, B. N. (1999). Upper Triassic Takla Group volcanic rocks, Stikine
1104 terrane, north-central British Columbia: geochemistry, petrogenesis, and tectonic implications,
1105 *Canadian Journal of Earth Sciences, 36*, 1483-1494.

1106 Dostal, J., Church, B. N., & Hoy, T. (2001). Geological and geochemical evidence for variable
1107 magmatism and tectonics in the southern Canadian Cordillera: Paleozoic to Jurassic suites,
1108 Greenwood, southern British Columbia, *Canadian Journal of Earth Sciences, 38*, 75-90.
1109 Draut, A. E., & Clift, P. D. (2012). Basins in arc-continent collisions, In Busby, C., & Azor, A. (Eds.),
1110 *Tectonics of Sedimentary Basins: Recent Advances* (pp. 347-368): Blackwell Publishing Ltd.
1111 Dusel-Bacon, C., Aleinikoff, J. N., Day, W. C., & Mortensen, J. K. (2015). Mesozoic magmatism and
1112 timing of epigenetic Pb-Zn-Ag mineralization in the western Fortymile mining district, east-
1113 central Alaska: Zircon U-Pb geochronology, whole-rock geochemistry, and Pb isotopes,
1114 *Geosphere, 11*, 786-822.
1115 Dyer, S. (2020). *The Early Jurassic metamorphic history of the Yukon-Tanana terrane of northwestern*
1116 *British Columbia: Insights from a new inverse garnet fractionation modelling technique* (M.Sc.
1117 thesis). Ottawa, ON: Carleton University.
1118 English, J. M., Johannson, G. G., Johnston, S. T., Mihalynuk, M. G., Fowler, M., & Wight, K. L. (2005).
1119 Structure, stratigraphy and petroleum resource potential of the central Whitehorse trough,
1120 northern Canadian Cordillera, *Bulletin of Canadian Petroleum Geology, 53*, 130-153.
1121 Erdmer, P., Ghent, E. D., Archibald, D. A., & Stout, M. Z. (1998). Paleozoic and Mesozoic high-
1122 pressure metamorphism at the margin of ancestral North America in central Yukon, *Geological*
1123 *Society of America Bulletin, 110*, 615-629.
1124 Evenchick, C. A. (1988). *Stratigraphy, metamorphism, structure, and their tectonic implications in the*
1125 *Sifton and Deserters Ranges, Cassiar and Northern Rocky Mountains, northern British*
1126 *Columbia* (Bulletin 376). Ottawa, ON: Geological Survey of Canada.

1127 Evenchick, C. A., Poulton, T. P., & McNicoll, V. J. (2010). Nature and significance of the diachronous
1128 contact between the Hazelton and Bowser Lake groups (Jurassic), north-central British
1129 Columbia, *Bulletin of Canadian Petroleum Geology, 58*, 235-267.
1130 Evenchick, C. A., McMechan, M. E., McNicoll, V. J., & Carr, S. D. (2007). A synthesis of the Jurassic–
1131 Cretaceous tectonic evolution of the central and southeastern Canadian Cordillera: Exploring
1132 links across the orogen, In Sears, J. W., Harms, T. A., & Evenchick, C. A. (Eds.), *Whence the*
1133 *Mountains? Inquiries into the Evolution of Orogenic Systems: A Volume in Honor of Raymond*
1134 *A. Price, Special Paper* (433, pp. 117-145): Boulder, CO: Geological Society of America.
1135 Ferri, F. (1997). Nina Creek Group and Lay Range Assemblage, north-central British Columbia:
1136 remnants of late Paleozoic oceanic and arc terranes, *Canadian Journal of Earth Sciences, 34*,
1137 854-874.
1138 Frazer, R. E., Coleman, D. S., & Mills, R. D. (2014). Zircon U-Pb geochronology of the Mount Givens
1139 Granodiorite: Implications for genesis of large volumes of eruptible magma, *Journal of*
1140 *Geophysical Research, Solid Earth, 119*, 2907-2924, https://10.1002/2013JB010716.
1141 Gabrielse, H. (1985). Major dextral transcurrent displacements along the northern Rocky Mountain
1142 Trench and related lineaments in north-central British Columbia, *Geological Society of America*
1143 *Bulletin, 96*, 1-14.
1144 Gabrielse, H. (1998). *Geology of Cry Lake and Dease Lake map areas, north-central British Columbia*
1145 (Bulletin 504). Ottawa, ON: Geological Survey of Canada.
1146 Gabrielse, H., Murphy, D. C., & Mortensen, J. K. (2006). Cretaceous and Cenozoic dextral orogen-
1147 parallel displacements, magmatism and paleogeography, north-central Canadian Cordillera, In
1148 Haggart, J. W., Monger, J. W. H., & Enkin, R. J. (Eds.), *Paleogeography of the North American*

Cordillera: Evidence For and Against Large-Scale Displacements, Special Paper (46, pp. 255-276): St. John's, NL: Geological Association of Canada.

Gagnon, J.-F., Evenchick, C. A., Waldron, J. W. F., Cordey, F., & Poulton, T. P. (2009). Jurassic subsidence history of the Hazelton Trough - Bowser Basin in the area of Todagin Mountain, north-central British Columbia, Canada, *Bulletin of Canadian Petroleum Geology, 57*, 430-448.

Gagnon, J.-F., Baressi, T., Waldron, J. W. F., Nelson, J. L., Poulton, T. P., & Cordey, F. (2012). Stratigraphy of the upper Hazelton Group and the Jurassic evolution of the Stikine terrane, British Columbia, *Canadian Journal of Earth Sciences, 49*, 1027-1052.

Gaidies, F., Morneau, Y. E., Petts, D. C., Jackson, S. E., Zagorevski, A., & Ryan, J. J. (2021). Major and trace element mapping of garnet: Unravelling the conditions, timing and rates of metamorphism of the Snowcap assemblage, west-central Yukon, *Journal of metamorphic Geology, 39*, 133-164, https://10.1111/jmg.12562.

George, S. W. M., Nelson, J. L., Alberts, D., Greig, C. J., & Gehrels, G. E. (2021). Triassic–Jurassic accretionary history and tectonic origins of Stikinia from U-Pb geochronology and Lu-Hf isotope analysis, British Columbia, *Tectonics, 40*, e2020TC006505, https://doi.org/10.1029/2020TC006505.

Gilotti, J. A., McClelland, W. C., van Staal, C. R., & Petrie, M. B. (2017). Detrital zircon evidence for eclogite formation by basal subduction erosion – An example from the Yukon-Tanana composite arc, Canadian Cordillera, In Bianchini, G., Bodinier, J.-L., Braga, R., & Wilson, M. (Eds.), *The Crust-Mantle and Lithosphere-Asthenosphere Boundaries: Insights from Xenoliths, Orogenic Deep Sections, and Geophysical Studies, Special Paper* (526, pp. 173-189): Boulder, CO: Geological Society of America.

1171 Glazner, A. F., Bartley, J. M., Coleman, D. S., Gray, W., & Taylor, R. Z. (2004). Are plutons assembled
1172 over millions of years by amalgamation from small magma chambers?, *GSA Today, 14, no. 4/5*,
1173 4-11.
1174 Golding, M. L., Mortensen, J. K., Ferri, F., Zonneveld, J.-P., & Orchard, M. J. (2016). Determining the
1175 provenance of Triassic sedimentary rocks in northeastern British Columbia and western Alberta
1176 using detrital zircon geochronology, with implications for regional tectonics, *Canadian Journal*
1177 *of Earth Sciences, 53*, 140-155.
1178 Goldstein, S. L., O'Nions, R. K., & Hamilton, P. J. (1984). A Sm-Nd isotopic study of atmospheric
1179 dusts and particulates from major river systems, *Earth and Planetary Science Letters, 70*, 221-
1180 236.
1181 Gordey, S. P., & Makepeace, A. J. (2001). *Bedrock geology, Yukon Territory* (Open File 3754). Ottawa,
1182 ON: Geological Survey of Canada.
1183 Greig, C. J. (2014). Latest Triassic-earliest Jurassic contractional deformation, uplift and erosion in
1184 Stikinia, NW B.C. In *Annual meeting*, *Abstracts with Programs*, (Vol. 46, pp. 588). Vancouver,
1185 B.C.: Geological Society of America.
1186 Greig, C. J., & Gehrels, G. E. (1995). U-Pb zircon geochronology of Lower Jurassic and Paleozoic
1187 Stikinian strata and Tertiary intrusions, northwestern British Columbia, *Canadian Journal of*
1188 *Earth Sciences, 32*, 1155-1171.
1189 Gunning, M. H., Hodder, R. W. H., & Nelson, J. L. (2006). Contrasting volcanic styles and their tectonic
1190 implications for the Paleozoic Stikine assemblage, western Stikine terrane, northwestern British
1191 Columbia, In Colpron, M., & Nelson, J. L. (Eds.), *Paleozoic Evolution and Metallogeny of*
1192 *Pericratonic Terranes at the Ancient Pacific Margin of North America, Canadian and Alaskan*
1193 *Cordillera, Special Paper* (45, pp. 201-227): St. John's, NL: Geological Association of Canada.

1194 Hammarstrom, J. M., & Zen, E. A. (1986). Aluminum in hornblende: an empirical igneous
1195 geobarometer, *American Mineralogist, 71*, 1297-1313.
1196 Han, T., Ootes, L., & Yun, K. (2020). *The new British Columbia Geological Survey geochronologic*
1197 *database: Preliminary release of ages*. (GeoFile 2020-10). Victoria, BC: British Columbia
1198 Ministry of Energy, Mines and Petroleum Resources, British Columbia Geological Survey.
1199 Harris, M. J., Symons, D. T. A., Blackburn, W. H., Hart, C. J. R., & Villeneuve, M. E. (2003). Travels
1200 of the Cache Creek terrane: a paleomagnetic. geobarometric and $^{40}Ar/^{39}Ar$ study of the Fourth of
1201 July batholith, Canadian Cordillera, *Tectonophysics, 362*, 137-159.
1202 Hart, C. J. R. (1995). *Magmatic and tectonic evolution of the Intermontane superterrane and Coast*
1203 *Plutonic complex in southern Yukon Territory* (M.Sc. thesis). Vancouver, BC: University of
1204 British Columbia.
1205 Hart, C. J. R. (1997). *A transect across northern Stikinia: Geology of the northern Whitehorse map area,*
1206 *southern Yukon Territory (105D/13-16)*. Whitehorse, YT: Yukon Geological Survey.
1207 Hart, C. J. R., Dickie, J. R., Ghosh, D. K., & Armstrong, R. L. (1995). Provenance constraints for
1208 Whitehorse Trough conglomerate: U-Pb zircon dates and initial Sr ratios of granitic clasts in
1209 Jurassic Laberge Group, Yukon Territory, In Miller, D. M., & Busby, C. (Eds.), *Jurassic*
1210 *Magmatism and Tectonics of the North American Cordillera, Special Paper* (299, pp. 47-63).
1211 Boulder, CO: Geological Society of America.
1212 Hodges, K. (2014). Thermochronology in orogenic systems, In Turekian, H. D. H. K. (Eds.), *Treatise on*
1213 *Geochemistry, 2nd edition* (pp. 281-308). Oxford, UK: Elsevier.
1214 Hood, S. B. (2012). *Mid-crustal Cu-Au mineralization during episodic pluton emplacement,*
1215 *hydrothermal fluid flow, and ductile deformation at the Minto deposit, YT, Canada* (M.Sc.
1216 thesis). Vancouver, BC: University of British Columbia.

1217 Jackson, J. L., Gehrels, G. E., Patchett, P. J., & Mihalynuk, M. G. (1991). Stratigraphy and isotopic link
1218 between the northern Stikine terrane and an ancient continental margin assemblage, Canadian
1219 Cordillera, *Geology, 19*, 1177-1180.
1220 Johannson, G. G., Smith, P. L., & Gordey, S. P. (1997). Early Jurassic evolution of the northern
1221 Stikinian arc: Evidence from the Laberge Group, northwestern British Columbia, *Canadian*
1222 *Journal of Earth Sciences, 34*, 1030-1057.
1223 Jones, G., Ootes, L., Milidragovic, D., Friedman, R., Camacho, A., Luo, Y., Vezinet, A., Pearson, D. G.,
1224 & Schiarizza, P. (2021). Geochronology of northern Hogem batholith, Quesnel terrane, north-
1225 central British Columbia. In Geological Fieldwork 2020 (Paper 2021-1, pp. 37-56). Victoria, BC:
1226 British Columbia Ministry of Energy, Mines and Low Carbon Innovation, British Columbia
1227 Geological Survey.
1228 Joyce, N. L., Ryan, J. J., Colpron, M., Hart, C. J. R., & Murphy, D. C. (2015). *A compilation of $^{40}Ar/^{39}Ar$*
1229 *age determinations for igneous and metamorphic rocks, and mineral occurrences from central*
1230 *and southeast Yukon*. (Open File 7924). Ottawa, ON: Geological Survey of Canada.
1231 Kay, R. W., & Kay, S. M. (1993). Delamination and delamination magmatism, *Tectonophysics, 219*,
1232 177-189.
1233 Kellett, D. A., & Iraheta Muniz, P. (2019). *Detrital U-Pb zircon and $^{40}Ar/^{39}Ar$ muscovite geochronology*
1234 *of the Whitehorse trough, and surrounding rocks, Yukon and British Columbia*. (Open File
1235 8565). Ottawa, ON: Geological Survey of Canada.
1236 Kellett, D. A., Weller, O. M., Zagorevski, A., & Regis, D. (2018). A petrochronological approach for the
1237 detrital record: Tracking mm-sized eclogite clasts in the northern Canadian Cordillera, *Earth and*
1238 *Planetary Science Letters, 494*, 23-31, https://doi.org/10.1016/j.epsl.2018.04.036.

1239 Kent, D. V., & Irving, E. (2010). Influence of inclination error in sedimentary rocks on the Triassic and
1240 Jurassic apparent pole wander path for North America and implications for Cordilleran tectonics,
1241 *Journal of Geophysical Research, 115*, 1-25.
1242 Klöcking, M., Mills, L., Mortensen, J. K., & Roots, C. F. (2016). *Geology of mid-Cretaceous volcanic*
1243 *rocks at Mount Nansen, central Yukon, and their relationship to the Dawson Range batholith*.
1244 (Open File 2016-25). Whitehorse, YT: Yukon Geological Survey.
1245 Knight, E., Schneider, D. A., & Ryan, J. J. (2013). Thermochronology of the Yukon-Tanana terrane,
1246 west-central Yukon: Evidence for Jurassic extension and exhumation in the northern Cordillera,
1247 *Journal of Geology, 121*, 371-400.
1248 Kovacs, N., Allan, M. M., Crowley, J. L., Colpron, M., Hart, C. J. R., Zagorevski, A., & Creaser, R. A.
1249 (2020). Carmacks Copper Cu-Au-Ag deposit: mineralization and post-ore migmatization of a
1250 Stikine arc porphyry copper system in Yukon, Canada, *Economic Geology, 115*, 1413-1442.
1251 Labails, C., Olivet, J.-L., Aslanian, D., & Roest, W. R. (2010). An alternative early opening scenario for
1252 the Central Atlantic Ocean, *Earth and Planetary Science Letters, 297*, 355-368.
1253 Le Bas, M. J., & Streckeisen, A. L. (1991). The IUGS systematics of igneous rocks, *Journal of the*
1254 *Geological Society, London, 148*, 825–833.
1255 Le Bas, M. J., Le Maitre, R. W., Streckeisen, A., & Zanettin, B. (1986). A chemical classification of
1256 volcanic rocks based on the total alkalis-silica diagram, *Journal of Petrology, 27*, 745-750.
1257 Logan, J. M., & Mihalynuk, M. G. (2014). Tectonic controls on Early Mesozoic paired alkaline
1258 porphyry deposit belts (Cu-Au ± Ag-Pt-Pd-Mo) within the Canadian Cordillera, *Economic*
1259 *Geology, 109*, 827-858.
1260 Logan, J. M., Moynihan, D. P., & Diakow, L. J. (2012). Dease Lake Geoscience Project, Part I: Geology
1261 and Mineralization of the Dease Lake (NTS 104J/08) and East-Half of the Little Tuya River

(NTS 104J/07E) Map Sheets, Northern British Columbia, *Geological Fieldwork 2011*. (Paper 2012-1, pp. 23-44). Victoria, B.C.: British Columbia Ministry of Energy, Mines and Petroleum Resources, British Columbia Geological Survey.

Logan, J. M., Drobe, J. R., & McClelland, W. C. (2000). *Geology of the Forrest Kerr - Mess Creek area, northwestern British Columbia (NTS 104B/10, 15 & 104G/2 & 7W)*. (Bulletin 104). British Columbia Ministry of Energy and Mines, British Columbia Geological Survey.

Long, D. G. F. (2015). *Depositional and tectonic framework of braided and meandering gravel-bed river deposits and associated coal deposits in active intermontane basins: The Upper Jurassic to mid-Cretaceous Tantalus Formation, Whitehorse trough, Yukon, Canada*. (Open File 2015-23). Whitehorse, YT: Yukon Geological Survey.

Lowey, G. W. (2008). Summary of the stratigraphy, sedimentology and hydrocarbon potential of the Laberge Group (Lower-Middle Jurassic), Whitehorse trough, Yukon, In Emond, D. S., Blackburn, L. R., Hill, R. P., & Weston, L. H. (Eds.), *Yukon Exploration and Geology 2007* (pp. 179-197): Whitehorse, YT: Yukon Geological Survey.

Marsden, H., & Thorkelson, D. J. (1992). Geology of the Hazelton volcanic belt in British Columbia: Implications for the Early to Middle Jurassic evolution of Stikinia, *Tectonics, 11*, 1266-1287.

McCartney, T. M. (2012). *A methodology for studying tectonic subsidence variations: Insight from the Fernie Formation of west-central Alberta* (M.Sc. thesis). University of Calgary.

McCausland, P. J. A., Symons, D. T. A., Hart, C. J. R., & Blackburn, W. H. (2002). Paleomagnetism and geobarometry of the Granite Mountain batholith, Yukon: Minimal geotectonic motion of the Yukon-Tanana terrane relative to North America, In Emond, D. S., Weston, L. H., & Lewis, L. L. (Eds.), *Yukon Exploration and Geology 2001* (pp. 163-177): Whitehorse, YT: Yukon Geological Survey.

McGoldrick, S., Zagorevski, A., & Canil, D. (2017). Geochemistry of volcanic and plutonic rocks from the Nahlin ophiolite with implications for a Permo-Triassic arc in the Cache Creek terrane, northwestern British Columbia, *Canadian Journal of Earth Sciences, 54*, 1214-1227.

Mihalynuk, M. G., Nelson, J., & Diakow, L. J. (1994). Cache Creek terrane entrapment: Oroclinal paradox within the Canadian Cordillera, *Tectonics, 13*, 575-595.

Mihalynuk, M. G., Erdmer, P., Ghent, E. D., Cordey, F., Archibald, D. A., Friedman, R. M., & Johannson, G. G. (2004). Coherent French Range blueschist: Subduction to exhumation in <2.5 m.y.?, *Geological Society of America Bulletin, 116*, 910-922.

Mihalynuk, M. G., Mountjoy, K. J., Smith, M. T., Currie, L. D., Gabites, J. E., Tipper, H. W., Orchard, M. J., Poulton, T. P., & Cordey, F. (1999). *Geology and mineral resources of the Tagish Lake area (NTS 104M/8, 9, 10E, 15 and 104N/12W), northwestern British Columbia*. (Bulletin 105). Victoria, B.C.: British Columbia Ministry of Energy and Mines, British Columbia Geological Survey.

Mihalynuk, M. G., Smith, M. T., Gabites, J. E., Runkle, D., & Lefebure, D. (1992). Age of emplacement and basement character of the Cache Creek terrane as constrained by new isotopic and geochemical data, *Canadian Journal of Earth Sciences, 29*, 2463-2477.

Mihalynuk, M. G., Zagorevski, A., Milidragovic, D., Tsekhmistrenko, M., Friedman, R. M., Joyce, N., Camacho, A., & Golding, M. L. (2018). Geologic and geochronologic update of the Turtle Lake area, NTS 104M/16, northwest British Columbia(Eds.), *Geological Fieldwork 2017*. (Paper 2018-1, pp. 83-128). Victoria, BC: British Columbia Ministry of Energy, Mines and Petroleum Resources, British Columbia Geological Survey.

Monger, J. W. H. (1977). Upper Paleozoic rocks of the western Canadian Cordillera and their bearing on Cordilleran evolution, *Canadian Journal of Earth Sciences, 14*, 1832-1859.

1308 Monger, J. W. H., & Ross, C. A. (1971). Distribution of fusulinaceans in the western Canadian
1309 Cordillera, *Canadian Journal of Earth Sciences, 8*, 259-278.
1310 Monger, J. W. H., & Nokleberg, W. J. (1996). Evolution of the northern North American Cordillera:
1311 generation, fragmentation, displacement and accretion of successive North American plate-
1312 margin arcs, In Coyner, A. R., & Fahey, P. L. (Eds.), *Geology and Ore Deposits of the American*
1313 *Cordillera Symposium Proceedings* (III, pp. 1133-1152). Reno/Sparks, NV: Geological Society
1314 of Nevada.
1315 Monger, J. W. H., & Price, R. A. (2002). The Canadian Cordillera: Geology and tectonic evolution,
1316 *Canadian Society of Exploration Geophysicists Recorder, 27*, 17-36.
1317 Monger, J. W. H., & Gibson, H. D. (2019). Mesozoic-Cenozoic deformation in the Canadian Cordillera:
1318 The record of a "Continental Bulldozer"?, *Tectonophysics, 757*, 153-169.
1319 Monger, J. W. H., Price, R. A., & Tempelman-Kluit, D. J. (1982). Tectonic accretion and the origin of
1320 two metamorphic and plutonic welts in the Canadian Cordillera, *Geology, 10*, 70-75.
1321 Mortensen, J. K. (1990). Geology and U-Pb geochronology of the Klondike District, west-central
1322 Yukon, *Canadian Journal of Earth Sciences, 27*, 903-914.
1323 Mortensen, J. K. (1992). Pre-Mid-Mesozoic tectonic evolution of the Yukon-Tanana terrane, Yukon and
1324 Alaska, *Tectonics, 11*, 836-853.
1325 Mortensen, J. K., & Jilson, G. A. (1985). Evolution of the Yukon-Tanana terrane: evidence from
1326 southeastern Yukon Territory, *Geology, 13*, 806-810.
1327 Mortensen, J. K., Ghosh, D., & Ferri, F. (1995). U-Pb age constraints of intrusive rocks associated with
1328 copper-gold porphyry deposits in the Canadian Cordillera, In Schroeter, T. G. (Ed.), *Porphyry*
1329 *deposits of the northwestern Cordillera of North America* (Special Volume 46, pp. 142-158):
1330 Canadian Institute of Mining and Metallurgy.

1331 Murphy, D. C., van der Heyden, P., Parrish, R. R., Klepacki, D. W., McMillan, W., Struik, L. C., &
1332 Gabites, J. (1995). New geochronological constraints on Jurassic deformation of the western
1333 edge of North America, southeastern Canadian Cordillera, In Miller, D. M., & Busby, C. (Eds.),
1334 *Jurassic Magmatism and Tectonics of the North American Cordillera, Special Paper* (299, pp.
1335 159-171): Boulder, CO: Geological Society of America.
1336 Nelson, J. L., & Mihalynuk, M. G. (1993). Cache Creek ocean: closure or enclosure?, *Geology, 21*, 173-
1337 176.
1338 Nelson, J. L., & Friedman, R. M. (2004). Superimposed Quesnel (late Paleozoic-Jurassic) and Yukon-
1339 Tanana (Devonian-Mississippian) arc assemblages, Cassiar Mountains, northern British
1340 Columbia: field, U-Pb and igneous petrochemical evidence, *Canadian Journal of Earth Sciences,*
1341 *41*, 1201-1235.
1342 Nelson, J. L., & Colpron, M. (2007). Tectonics and metallogeny of the Canadian and Alaskan
1343 Cordillera, 1.8 Ga to present, In Goodfellow, W. D. (Ed.), *Mineral Deposits of Canada: A*
1344 *Synthesis of Major Deposit Types, District Metallogeny, the Evolution of Geological Provinces,*
1345 *and Exploration Methods, Special Publication* (5, pp. 755-791). St. John's, NL: Geological
1346 Association of Canada, Mineral Deposit Division.
1347 Nelson, J. L., Colpron, M., & Israel, S. (2013). The Cordillera of British Columbia, Yukon, and Alaska:
1348 Tectonics and metallogeny, In Colpron, M., Bissig, T., Rusk, B. G., & Thompson, J. F. H. (Eds.),
1349 *Tectonics, Metallogeny and Discovery: The North American Cordillera and Similar*
1350 *Accretionary Settings* (Special Publication 17, pp. 53-103). Littleton, CO: Society of Economic
1351 Geologists, Inc.

Nelson, J. L., van Straaten, B., & Friedman, R. (2022). Latest Triassic-Early Jurassic Stikine – Yukon-Tanana terrane collision and the onset of accretion in the Canadian Cordillera: insights from Hazelton Group detrital zircon provenance and arc–back-arc configuration, *Geosphere* (in press).

Nelson, J. L., Waldron, J. W. F., van Straaten, B., Zagorevski, A., & Rees, C. J. (2018). Revised stratigraphy of the Hazelton Group in the Iskut River region, northwestern British Columbia, *Geological Fieldwork 2017* (Paper 2018-1, pp. 15-38): Victoria, BC: British Columbia Ministry of Energy, Mines and Petroleum Resources, British Columbia Geological Survey.

Nelson, J. L., Colpron, M., Piercey, S. J., Dusel-Bacon, C., Murphy, D. C., & Roots, C. F. (2006). Paleozoic tectonic and metallogenic evolution of the pericratonic terranes in Yukon, northern British Columbia and eastern Alaska, In Colpron, M., & Nelson, J. L. (Eds.), *Paleozoic Evolution and Metallogeny of Pericratonic Terranes at the Ancient Pacific Margin of North America, Canadian and Alaskan Cordillera, Special Paper* (45, pp. 323-360). St. John's, NL: Geological Association of Canada.

Nixon, G. T., Scheel, J. E., Scoates, J. S., Friedman, R. M., Wall, C. J., Gabites, J., & Jackson-Brown, S. (2020). Syn-accretionary multistage assembly of an Early Jurassic Alaskan-type intrusion in the Canadian Cordillera: U-Pb and $^{40}Ar/^{39}Ar$ geochronology of the Turnagain ultramafic-mafic intrusive complex, Yukon-Tanana terrane, *Canadian Journal of Earth Sciences, 57*, 575-600.

Nixon, G. T., Hammack, J. L., Ash, C. H., Cabri, L. J., Case, G., Connelly, J. N., Heaman, L. M., Laflamme, J. H. G., Nuttall, C., Paterson, W. P. E., & Wong, R. H. (1997). *Geology and platinum-group-element mineralization of Alaskan-type ultramafic-mafic complexes in British Columbia*. (Bulletin 93). Victoria, BC: British Columbia Ministry of Energy and Mines, British Columbia Geological Survey.

1374 Pană, D. I., Poulton, T. P., & DuFrane, S. A. (2018). U-Pb detrital zircon dating supports Early Jurassic
1375 initiation of the Cordilleran foreland basin in southwestern Canada, *Geological Society of*
1376 *America Bulletin, 131*, 318-334.
1377 Parsons, A. J., Coleman, M. J., Ryan, J. J., Zagorevski, A., Joyce, N. L., Gibson, H. D., & Larson, K. P.
1378 (2018). Structural evolution of a crustal-scale shear zone through a decreasing temperature
1379 regime: The Yukon River shear zone, Yukon-Tanana terrane, Northern Cordillera, *Lithosphere,*
1380 *10*, 760-782.
1381 Peccerillo, A., & Taylor, S. R. (1976). Geochemistry of calc-alkaline volcanic rocks from the
1382 Kastamonu area, Northern Turkey, *Contributions to Mineralogy and Petrology, 58*, 63-81.
1383 Pecha, M. E., Gehrels, G. E., McClelland, W. C., Giesler, D., White, C., & Yokelson, I. (2016). Detrital
1384 zircon U-Pb geochronology and Hf isotope geochemistry of the Yukon-Tanana terrane, Coast
1385 Mountains, southeast Alaska, *Geosphere, 12*, 1556-1574.
1386 Petrie, M. B., Massonne, H.-J., Gilotti, J. A., McClelland, W. C., & van Staal, C. R. (2016). The P-T
1387 path of eclogite in the St. Cyr klippe, Yukon, Canada: Permian metamorphism of a coherent
1388 high-pressure unit in an accreted terrane of the North American Cordillera, *European Journal of*
1389 *Mineralogy, 28*, 1111-1130.
1390 Piercey, S. J., & Colpron, M. (2009). Composition and provenance of the Snowcap assemblage,
1391 basement to the Yukon-Tanana terrane, northern Cordillera: Implications for Cordilleran crustal
1392 growth, *Geosphere, 5*, 439-464, https://10.1130/GES00505.1.
1393 Piercey, S. J., Nelson, J. L., Colpron, M., Dusel-Bacon, C., Roots, C. F., & Simard, R.-L. (2006).
1394 Paleozoic magmatism and crustal recycling along the ancient Pacific margin of North America,
1395 northern Cordillera, In Colpron, M., & Nelson, J. L. (Eds.), *Paleozoic Evolution and*
1396 *Metallogeny of Pericratonic Terranes at the Ancient Pacific Margin of North America,*

Canadian and Alaskan Cordillera, Special Paper (45, pp. 281-322). St. John's, NL: Geological Association of Canada.

Read, P. B., Woodsworth, G. J., Greenwood, H. J., Ghent, E. D., & Evenchick, C. A. (1991). *Metamorphic map of the Canadian Cordillera* (Map 1714A). Ottawa, ON: Geological Survey of Canada.

Roots, C. F., Nelson, J. L., Simard, R.-L., & Harms, T. A. (2006). Continental fragments, mid-Paleozoic arcs and overlapping late Paleozoic arc and Triassic sedimentary strata in the Yukon-Tanana terrane of northern British Columbia and southern Yukon, In Colpron, M., & Nelson, J. L. (Eds.), *Paleozoic Evolution and Metallogeny of Pericratonic Terranes at the Ancient Pacific Margin of North America, Canadian and Alaskan Cordillera, Special Paper* (45, pp. 153-177). St. John's, NL: Geological Association of Canada.

Roots, C. F., Nelson, J. L., Mihalynuk, M. G., Harms, T. A., de Keijzer, M., & Simard, R.-L. (2004). *Bedrock geology, Dorsey Lake (NTS 105B/4), southern Yukon (1:50,000 scale)* (Open File 2004-2). Whitehorse, YT: Yukon Geological Survey.

Ross, C. A., & Monger, J. W. H. (1978). Carboniferous and Permian fusulinaceans from the Omineca Mountains, British Columbia, In Donnelly, V. (Ed.), *Contributions to Canadian Paleontology* (Bulletin 267, pp. 43-63). Ottawa, ON: Geological Survey of Canada.

Rudnick, R. L. (1995). Making continental crust, *Nature, 378*, 571-578.

Ruks, T. W., Piercey, S. J., Ryan, J. J., Villeneuve, M. E., & Creaser, R. A. (2006). Mid- to late Paleozoic K-feldspar augen granitoids of the Yukon-Tanana terrane, Yukon, Canada: Implications for crustal growth and tectonic evolution of the northern Cordillera, *Geological Society of America Bulletin, 118*, 1212-1231, https://10.1130/B25854.1.

1419 Ryan, J. J., Zagorevski, A., Roots, C. F., & Joyce, N. (2014). *Paleozoic tectonostratigraphy of the*
1420 *northern Stevenson Ridge area, Yukon*. (Current Research 2014-4). Ottawa, ON: Geological
1421 Survey of Canada.
1422 Ryan, J. J., Zagorevski, A., Williams, S. P., Roots, C. F., Ciolkiewicz, W., Hayward, N., & Chapman, J.
1423 B. (2013). *Geology, Stevenson Ridge (northeast part), Yukon* (Canadian Geoscience Map 116).
1424 Ottawa, ON: Geological Survey of Canada.
1425 Sack, P. J., Colpron, M., & Crowley, J. L. (2022). *U-Pb zircon geochronology from a Late Triassic*
1426 *pluton in the Mount Nansen area*. (Open File 2022-2). Whitehorse, YT: Yukon Geological
1427 Survey.
1428 Sack, P. J., Colpron, M., Crowley, J. L., Ryan, J. J., Allan, M. M., Beranek, L. P., Joyce, N. L.,
1429 Mortensen, J. K., Israel, S., & Chapman, J. B. (2020). *Atlas of Late Triassic to Jurassic plutons*
1430 *in the Intermontane terranes of Yukon*. (Open File 2020-1). Whitehorse, YT: Yukon Geological
1431 Survey. http://data.geology.gov.yk.ca/Reference/95839.
1432 Schellart, W. P., Freeman, J., Stegman, D. R., & May, D. (2007). Evolution and diversity of subduction
1433 zones controlled by slab width, *Nature, 446*, 308-311, https://doi:1038/nature05615.
1434 Schiarizza, P. (2012). Geology of the Kutcho assemblage between the Kehlechoa and Tucho Rivers,
1435 northern British Columbia (NTS 104I/01, 02), *Geological Fieldwork 2011*. (Paper 2012-1, pp.
1436 75-98). Victoria, BC: British Columbia Ministry of Energy, Mines and Petroleum Resources,
1437 British Columbia Geological Survey.
1438 Schmidt, M. W., & Poli, S. (2004). Magmatic epidote, In Liebscher, A., & Franz, G. (Eds.), *Epidotes.*
1439 *Reviews in Mineralogy and Geochemistry* (Vol. 56, pp. 399-430). Chantilly, VA: Mineralogical
1440 Society of America.

1441 Schneider, C. A., Rasband, W. S., & Eliceiri, K. W. (2012). NIH Image to ImageJ: 25 years of image
1442 analysis, *Nature Methods, 9*, 671-675.
1443 Schwartz, J. J., Klepeis, K. A., Sadorski, J. F., Stowell, H. H., Tulloch, A. J., & Coble, M. A. (2017).
1444 The tempo of continental arc construction in the Mesozoic Median Batholith, Fiordland, New
1445 Zealand, *Lithosphere, 9*, 343-365, https://10.1130/L610.1.
1446 Shand, S. J. (1943). *Eruptive Rocks; Their Genesis, Composition, Classification, and Their Relation to*
1447 *Ore Deposits, with a Chapter on Meteorites*, 444 pp., Hafner Publishing Co., New York, NY.
1448 Shirmohammad, F., Smith, P. L., Anderson, R. G., & McNicoll, V. J. (2011). The Jurassic succession at
1449 Lisadele Lake (Tulsequah map area, British Columbia, Canada) and its bearing on the tectonic
1450 evolution of the Stikine terrane, *Volumina Jurassica, 9*, 43-60.
1451 Simard, R.-L. (2003). *Geological map of southern Semenof Hills (part of NTS 105E/1,7,8), south-central*
1452 *Yukon (1:50 000 scale)* (Open File 2003-12). Whitehorse, YT: Yukon Geological Survey.
1453 Simard, R.-L., & Devine, F. (2003). Preliminary geology of the southern Semenof Hills, central Yukon
1454 (105E/1,7,8), In Emond, D. S., & Lewis, L. L. (Eds.), *Yukon Exploration and Geology 2002* (pp.
1455 213-222). Whitehorse, YT: Yukon Geological Survey.
1456 Simard, R.-L., Dostal, J., & Roots, C. F. (2003). Development of late Paleozoic volcanic arcs in the
1457 Canadian Cordillera: an example from the Klinkit Group, northern British Columbia and
1458 southern Yukon, *Canadian Journal of Earth Sciences, 40*, 907-924.
1459 Smith, P. L. (2006). Paleobiogeography and Early Jurassic molluscs in the context of terrane
1460 displacement in western Canada, In Haggart, J. W., Enkin, R. J., & Monger, J. W. H. (Eds.),
1461 *Paleogeography of the North American Cordillera: Evidence for and against large-scale*
1462 *displacements*. *Special Paper* (46, pp. 81-94). St. John's, NL: Geological Association of Canada.

1463 Smith, P. L., Tipper, H. W., & Ham, D. M. (2001). Lower Jurassic Amaltheidae (Ammotina) in North
1464 America: paleobiogeography and tectonic implications, *Canadian Journal of Earth Sciences, 38*,
1465 1439-1449.
1466 Smith, T., Rosenbaum, G., & Gross, L. (2021). Formation of oroclines by buckling continental ribbons:
1467 Fact or fiction?, *Tectonophysics, 814*, 9, https://doi.org/10.1016/j.tecto.2021.228950.
1468 Souther, J. G. (1971). *Geology and mineral deposits of Tulsequah map-area, British Columbia*. (Memoir
1469 362). Ottawa, ON: Geological Survey of Canada.
1470 Stanley, G. D. J., & Senowbari-Daryan, B. (1999). Upper Triassic reef fauna from the Quesnel terrane,
1471 central British Columbia, Canada, *Journal of Paleontology, 73*, 787–802.
1472 Staples, R. D., Gibson, H. D., Colpron, M., & Ryan, J. J. (2016). An orogenic wedge model for
1473 diachronous deformation, metamorphism, and exhumation in the hinterland of the northern
1474 Canadian Cordillera, *Lithosphere, 8*, 165-184, https://10.1130/L472.1.
1475 Stevens, C. H. (1995). A giant Permian fusulinid from east-central Alaska with comparisons of all giant
1476 fusulinids in western North America, *Journal of Paleontology, 69*, 802-812.
1477 Sundell, K., Saylor, J. E., & Pecha, M. (2019). Provenance and recycling of detrital zircons from
1478 Cenozoic Altiplano strata and the crustal evolution of western South America from combined U-
1479 Pb and Lu-Hf isotopic analysis, In Horton, B. K., & Folguera, A. (Eds.), *Andean Tectonics* (pp.
1480 363-397): Elsevier.
1481 Tafti, R. (2005). *Nature and origin of the Early Jurassic Copper (-Gold) deposits at Minto and Williams*
1482 *Creek, Carmacks Copper belt, western Yukon: examples of deformed porphyry deposits* (M.Sc.
1483 thesis). Vancouver, B.C.: University of British Columbia.
1484 Tempelman-Kluit, D. J. (1984). *Geology, Laberge (105E) and Carmacks (105I), Yukon Territory* (Open
1485 File 1101). Ottawa, ON: Geological Survey of Canada.

1486 Tempelman-Kluit, D. J. (2009). *Geology of Carmacks and Laberge map areas, central Yukon:*
1487 *Incomplete draft manuscript on stratigraphy, structure and its early interpretation (ca. 1986)*.
1488 (Open File 5982). Ottawa, ON: Geological Survey of Canada.
1489 Tipper, H. W. (1978). Jurassic biostratigraphy, Cry Lake map area, British Columbia, In *Current*
1490 *Research* (Paper 78-1A, pp. 25–27). Ottawa, ON: Geological Survey of Canada.
1491 Tipper, H. W., & Richards, T. A. (1976). *Jurassic stratigraphy and history of north-central British*
1492 *Columbia*. (Bulletin 270). Ottawa, ON: Geological Survey of Canada.
1493 Topham, M. J., Allan, M. M., Mortensen, J. K., Hart, C. J. R., Colpron, M., & Sack, P. J. (2016). Crustal
1494 depth of emplacement of the Early Jurassic Aishihik and Tatchun batholiths, west-central Yukon,
1495 In MacFarlane, K. E., & Nordling, M. G. (Eds.), *Yukon Exploration and Geology 2015* (pp. 233-
1496 251): Whitehorse, YT: Yukon Geological Survey.
1497 Travers, W. B. (1978). Overturned Nicola and Ashcroft strata and their relation to the Cache Creek
1498 Group, southwestern Intermontane Belt, British Columbia, *Canadian Journal of Earth Sciences,*
1499 *15*, 99-116.
1500 Unterschutz, J. L. E., Creaser, R. A., Erdmer, P., Thompson, R. I., & Daughtry, K. L. (2002). North
1501 American margin origin of Quesnel terrane strata in the southern Canadian Cordillera: Inferences
1502 from geochemical and Nd isotopic characteristics of Triassic metasedimentary rocks, *Geological*
1503 *Society of America Bulletin, 114*, 462-475.
1504 van Drecht, L. (2019). *Detrital zircon U-Pb geochronology and Hf isotope geochemistry of the Laberge*
1505 *Group: synorogenic siliciclastic record of early Mesozoic crustal thickening and tectonic*
1506 *evolution of the Whitehorse trough in the northern Canadian Cordillera* (M.Sc. thesis). St.
1507 John's, NL: Memorial University of Newfoundland.

1508 Vervoot, J. D., Patchett, P. J., Blichert-Toft, J., & Albarède, F. (1999). Relationships between Lu-Hf and
1509 Sm-Nd isotopic systems in the global sedimentary system, *Earth and Planetary Science Letters,*
1510 *168*, 79-99.
1511 von Blanckenburg, F., & Davies, J. H. (1995). Slab breakoff: A model for syncollisional magmatism and
1512 tectonics in the Alps, *Tectonics, 14*, 120-131.
1513 Wernicke, B., & Klepacki, D. W. (1988). Escape hypothesis for the Stikine block, *Geology, 16*, 461-
1514 464.
1515 Wheeler, J. O. (1961). *Whitehorse map-area, Yukon Territory, 105D*. (Memoir 312). Ottawa, ON:
1516 Geological Survey of Canada.
1517 Wheeler, J. O., & McFeely, P. (1991). *Tectonic assemblage map of the Canadian Cordillera and*
1518 *adjacent parts of the United States of America* (Map 1712A). Ottawa, ON: Geological Survey of
1519 Canada.
1520 White, D., Colpron, M., & Buffett, G. (2012). Seismic and geological constraints on the structure of the
1521 northern Whitehorse trough, Yukon, Canada, *Bulletin of Canadian Petroleum Geology, 60*, 239-
1522 255.
1523 Wilson, F. H., Hults, C. P., Mull, C. G., & Karl, S. M. (2015). *Geologic Map of Alaska* (Scientific
1524 Investigation Map 3340). Reston, VA: U.S. Geological Survey.
1525 Woodsworth, G. J., Anderson, R. G., & Armstrong, R. L. (1991). Plutonic Regimes, Chapter 15, In
1526 Gabrielse, H., & Yorath, C. J. (Eds.), *Geology of the Cordilleran Orogen in Canada* (Geology of
1527 Canada, no. 4, pp. 491-531): Ottawa, ON: Geological Survey of Canada.
1528 Yukon Geological Survey (2020a). *Yukon Digital Bedrock Geology*.
1529 (http://datatest.geology.gov.yk.ca/Compilation/3). Whitehorse, YT: Yukon Geological Survey.

Yukon Geological Survey (2020b). *Yukon MINFILE – A database of mineral occurrences*. (http://datatest.geology.gov.yk.ca/Compilation/24). Whitehorse, YT: Yukon Geological Survey.

Yukon Geological Survey (2020c). *Yukon Geochronology – A database of Yukon isotopic age determinations*. (http://data.geology.gov.yk.ca/Compilation/22). Whitehorse, YT: Yukon Geological Survey.

Zen, E.-a., & Hammarstrom, J. M. (1984). Magmatic epidote and its petrologic significance, *Geology, 12*, 515-518.

Figure Captions

Figure 1. Late Triassic to Jurassic plutons and significant Cu ±Au(±Mo) porphyry deposits of the northern Cordillera. Selected producing mines are labeled. Simplified terrane map modified after Colpron and Nelson (2011). Plutons are from Cui et al. (2017) for British Columbia, Yukon Geological Survey (2020a) for Yukon, and Wilson et al. (2015) for Alaska. Selected porphyry deposits are from BC MINFILE (British Columbia Geological Survey, 2019) and Yukon MINFILE (Yukon Geological Survey, 2020b) databases. BB – Bowser basin; HB – Hogem batholith; Mt. – Mount; Mtn. – Mountain; NRMT – Northern Rocky Mountain Trench; SA – Stikine arch; SK – Skeena arch; TM – Taylor Mountain batholith; YTs – Yukon-Tanana south; WT – Whitehorse trough.

Figure 2. Distribution of Late Triassic to Jurassic plutons in the Intermontane terranes of southern Yukon. The names of plutons described in the Atlas of Sack et al. (2020) are indicated. General locations of Paleozoic (Takhini, Boswell) and Triassic (Lewes River, Semenof) assemblanges of Stikinia are also indicated. Terrane map is modified after Colpron and Nelson (2011). Plutons and distribution of Whitehorse trough strata are from Yukon Geological Survey

(2020a). Jurassic faults (red labels): NRT – Needlerock thrust; TF – Tadru fault; WLF – Willow Lake fault; YRF – Yukon River fault. Other abbreviations: Lk – lake; Mtn – mountain; R. – river.

Figure 3. Palinspastic map of Early to Middle Jurassic plutons in southern Yukon and northern British Columbia; after restoration of dextral displacements along the Cenozoic Tintina fault (~490 km) and Cretaceous Big Salmon–Teslin fault system (~130 km; BSTF). Displacement estimates from Gabrielse et al. (2006) and Nelson et al. (2013, p. 88). Restoration on the Tintina fault aligns the portions of the Yukon-Tanana and Slide Mountain terranes northeast of the fault with their counterparts in west-central Yukon. Displacement of the BSTF north of 61°N is inferred to be partitioned into splays of the d'Abbadie, Big Salmon, and Towhata faults (Fig. 2), which collectively account for ~125 km of dextral displacement (Nelson & Colpron, 2007; Nelson et al., 2013). Jurassic structures are shown as grey lines with red labels. Dots show the location of samples analyzed by CA-TIMS for this study (Table 1-2 and Appendix 4 in Sack et al., 2020). Ages are rounded for simplicity; see Sack et al. (2020, Table 1-2; 2022) for precise dates. Yellow dots indicate samples for which inherited zircon cores were analyzed by LA-ICPMS. Black star shows approximate location of the Early Jurassic Turnagain complex in northern British Columbia (T; Nixon et al., 2020). Black squares show approximate location of the towns of Atlin (A), Carmacks (C) and Whitehorse (W) for reference. The Aishihik and Coconino–Simpson Peak–Nome Lake (C-SP-NL) batholiths are labeled and discussed in the text.

Figure 4. Summary of new CA-TIMS dates constraining the age of Late Triassic and Jurassic plutonic suites in southern Yukon (Table 1-2 and Appendix 4 in Sack et al., 2020; and Appendix

2 in Sack et al., 2022). Interpreted ages and their 2σ errors are shown by black boxes. Colored boxes show the range for individual plutonic suites.

Figure 5. Compositional range of Late Triassic to Jurassic plutonic suites in the Intermontane terranes of Yukon. a) Simplified Quartz–Alkali-feldspar–Plagioclase plot (after Le Bas & Streckeisen, 1991). b) Total alkali vs. silica diagram for plutonic rocks (after Le Bas et al., 1986). c) K_2O vs. SiO_2 diagram of Peccerillo and Taylor (1976). d) Alumina saturation index of Shand (1943). Modal abundances from stained hand sample slabs and major element geochemistry from Sack et al. (2020, Appendix 8).

Figure 6. Plots of $^{87}Sr/^{86}Sr_i$ (a), εNd_t (b) and zircon εHf_t (c) vs. age for Late Triassic to Jurassic plutons in southern Yukon. Note the contrasting isotopic evolution from plutons west and east of the Big Salmon–Teslin fault system. Data from Sack et al. (2020, Table 1-4, Appendices 9 and 10). Whole rock Sr (a) and Nd (b) analyses were done on samples precisely dated by CA-TIMS while the Hf data in c was acquired by LA-ICPMS spot analyses of igneous zircons yielding a scatter of U-Pb dates. Grey circles in b are from volcanic and sedimentary rocks of the Stuhini and Laberge groups reported in Jackson et al. (1991). Note that the age of sandstone samples with subchondritic εNd_t were corrected using detrital zircon maximum depositional ages from nearby strata of the Laberge Group (Kellett & Iraheta Muniz, 2019). Contours for Hf isotopic data in c were generated using the HafniumPlotter routine of Sundell et al. (2019). Dash grey line shows the 95th percentile contour for detrital zircon from the Laberge Group (WT dz; van Drecht, 2019; n = 954). BSE – bulk silicate Earth; CHUR – chondritic uniform reservoir.

Figure 7. Distribution of $^{87}Sr/^{86}Sr_i$ (a) and εNd_t (b) values for Late Triassic and Jurassic plutons shown on palinspastic map from Figure 3. Isotopic data from Sack et al. (2020, Table 1-4). Data

for the southernmost Sr samples in **a** are from Currie (1994) for Early Jurassic plutons (Bennett suite; n = 2) and Mihalynuk et al. (1992) for the Middle Jurassic Fourth of July suite (n = 3).

Figure 8. Plot of total Al content (Al_{TOT}) of hornblende (a) and Pressure (b) vs. age for Late Triassic and Jurassic plutons in Yukon. Pressures calculated using the Al-in-hornblende geobarometer of Anderson and Smith (1995). Data is presented in Sack et al. (2020, Table 1-3 and Appendix 5). Depth estimated using a lithostatic gradient of ~3.7 km/kbar. Samples from previous studies are shown in grey; data from McCausland et al. (2002) and Tafti (2005).

Figure 9. Probability density plots for Phanerozoic dates and εHf_t data from inherited zircon cores analyzed by LA-ICPMS (Appendices 3 and 10 in Sack et al., 2020). a) Minto suite; b) Long Lake suite; c) Lokken suite; d) McGregor suite; e) composite plot for all analyses. The range of crystallization age (crystal.) from CA-TIMS dates for each suite (Fig. 4) is indicated by black bar at the young end of the age spectra. f) Plot of εHf_t vs. age for inherited zircon cores. Hatched, pink areas indicate ranges of εHf_t values for source units from the literature (or equivalent range for εNd_t data, calculated using equation of Vervoot et al., 1999). F – Finlayson assemblage, mafic rocks εNd_t (Creaser et al., 1997b; Piercey et al., 2006); K – Klondike assemblage, felsic rocks εNd_t (Ruks et al., 2006); Kt – Klinkit assemblage, mafic rocks εNd_t (Simard et al., 2003); M – Minto suite, zircon εHf_t (Sack et al., 2020; this study); P – Povoas formation, mafic rocks εHf_t (Bordet et al., 2019); SR – Simpson Range suite, granitoid rocks εNd_t (Piercey et al., 2006); YTs – Devonian detrital zircon εHf_t from Yukon-Tanana terrane of southeastern Alaska (Pecha et al., 2016).

Figure 10. a) Spatial distribution of crystallization pressure estimates from Al-in-hornblende geobarometry in Jurassic granitoid plutons (data from Table 1-3 in Sack et al., 2020) and Early

Jurassic peak pressures from regional metamorphic studies of the Yukon-Tanana terrane (Berman et al., 2007; Clark, 2017; Dyer, 2020; Gaidies et al., 2021). b) Mica cooling ages for metamorphic and igneous rocks of the Intermontane terranes in Yukon (data from compilation of the Yukon Geological Survey, 2020c) and northern British Columbia (data from compilation of Han et al., 2020). Jurassic cooling ages are highlighted by yellow circles with labels showing the range for cluster of ages. Hatched area in the hanging wall of the Willow Lake fault (WLF) indicates part of the Yukon-Tanana terrane that cooled in the Paleozoic (Knight et al., 2013; Colpron et al., 2015; Staples et al., 2016). Sample locations are shown on the palinspastic restoration from Figure 3. C – Carmacks.

Figure 11. Regional relationships of Early to Middle Jurassic sedimentary basins, volcanic and magmatic belts in the northern Intermontane terranes of Yukon and northern British Columbia. Palinspastic restoration as in Figure 3 with additional restoration of dextral displacement on the Cassiar-Kutcho (~50 km) and Kechika-Finlay (~195 km) faults following Gabrielse (1985), Evenchick (1988) and Gabrielse et al. (2006). Note that this map is rotated with modern-day North pointing to upper left. Heavy red line along the Skeena arch marks approximate location of the Hazelton subduction zone (teeth pointing to upper plate). Heavy black line with teeth indicates the western boundary of Quesnellia with Cache Creek and Stikinia, which follows the modern traces of the Big Salmon–Teslin fault system (BSTF). Heavy green lines are traces of inferred Early Jurassic sinistral transform faults. Purple diamonds show locations of Early Jurassic eclogite clasts in Laberge Group (Eclogite Ridge, ER) and Middle Jurassic blueschists in the French Range (FR), Cache Creek terrane.

Figure 12. Ranked plot of $^{206}Pb/^{238}U$ zircon ages for all Late Triassic to Jurassic igneous samples analyzed from the Intermontane terranes in Yukon (data from Yukon Geological Survey, 2020c).

Data points are shown with 2σ errors and color-coded according to analytical technique. Data for the Lokken suite, east of the BSTF, are shown separately at right. A probability density plot for ages from plutons west of the BSTF is shown in red at left (n = 92). The age ranges of plutonic suites determined from CA-TIMS dates (Fig. 4) are indicated by color boxes.

Figure 13. Schematic paleogeography and tectonic evolution of the Intermontane terranes and northwestern edge of North America in Late Triassic to Middle Jurassic. Schematic section across southern Yukon shown in upper right in b–d. Relative position of plutonic suites discussed in this paper are shown by red dots. Synorogenic clastic rocks are shown by yellow stippled pattern. Terrane labels: CC – Cache Creek; Ku – Kutcho (including Sitlika-Wineglass-Venables assemblages; Logan & Mihalynuk, 2014); PE – Peninsular; QN – Quesnellia; ST – Stikinia; WR – Wrangellia; YT – Yukon-Tanana. Fault labels in cross-sections: LwF – Lewellyn fault; NRT – Needlerock thrust; WLF – Willow Lake fault.

Figure 1.

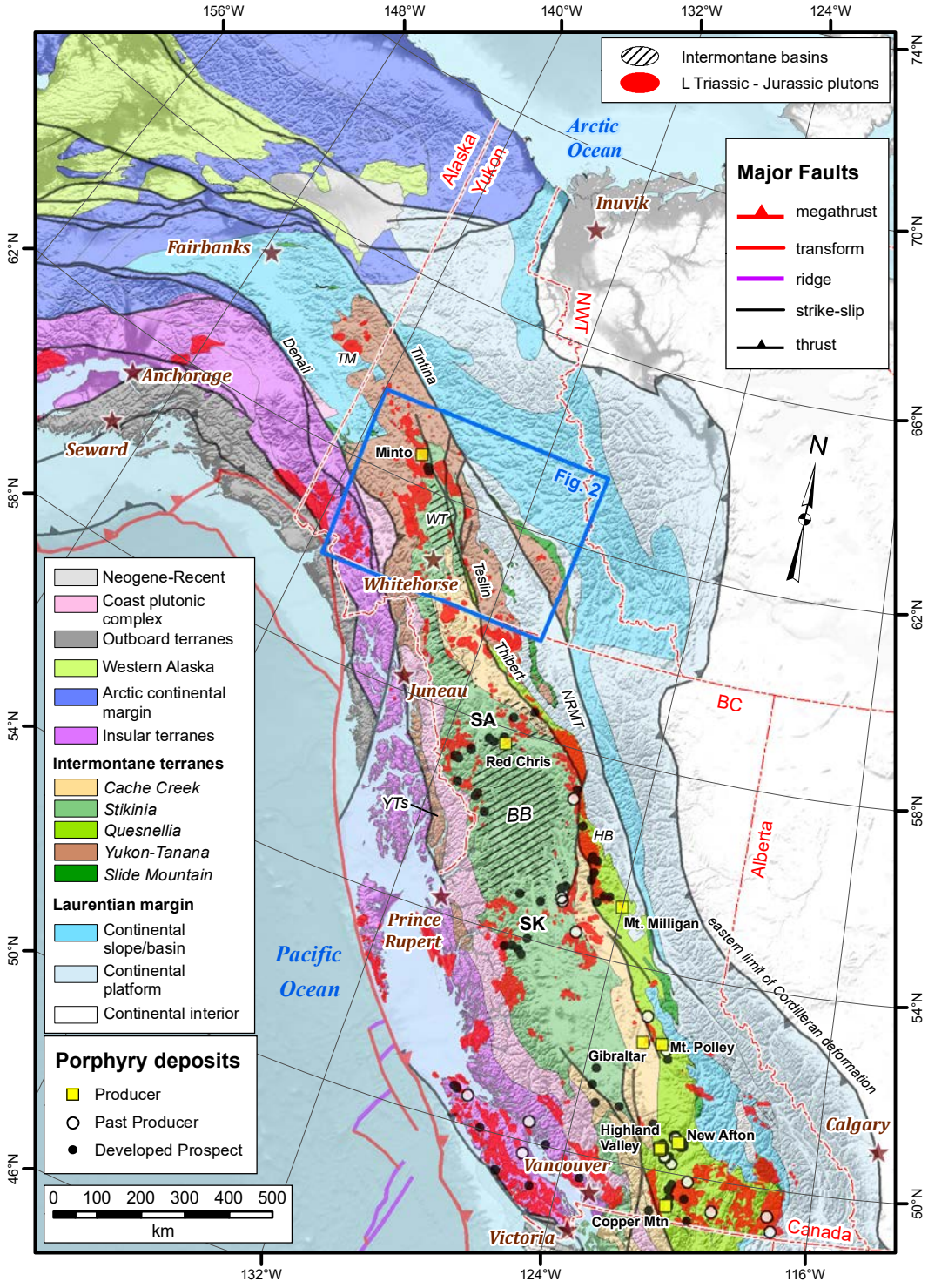
156°W
148°W
140°W
132°W
124°W
74°N
70°N
66°N
62°N
58°N
54°N
50°N
46°N
132°W
124°W
116°W
Intermontane basins
L Triassic - Jurassic plutons
Major Faults
megathrust
transform
ridge
strike-slip
thrust
Arctic Ocean
Alaska
Yukon
Inuvik
Fairbanks
NWT
Denali
TM
Tintina
Anchorage
Seward
Minto
Fig. 2
WT
Whitehorse
Tesslin
Thibert
NRMT
Juneau
SA
Red Chris
BC
YTs
BB
HB
Alberta
Prince Rupert
SK
Mt. Milligan
eastern limit of Cordilleran deformation
Pacific Ocean
Mt. Polley
Gibraltar
Highland Valley
New Afton
Calgary
Vancouver
Copper Mtn
Victoria
Canada
N
Neogene-Recent
Coast plutonic complex
Outboard terranes
Western Alaska
Arctic continental margin
Insular terranes
Intermontane terranes
Cache Creek
Stikinia
Quesnellia
Yukon-Tanana
Slide Mountain
Laurentian margin
Continental slope/basin
Continental platform
Continental interior
Porphyry deposits
Producer
Past Producer
Developed Prospect
0 100 200 300 400 500
km

Figure 2.

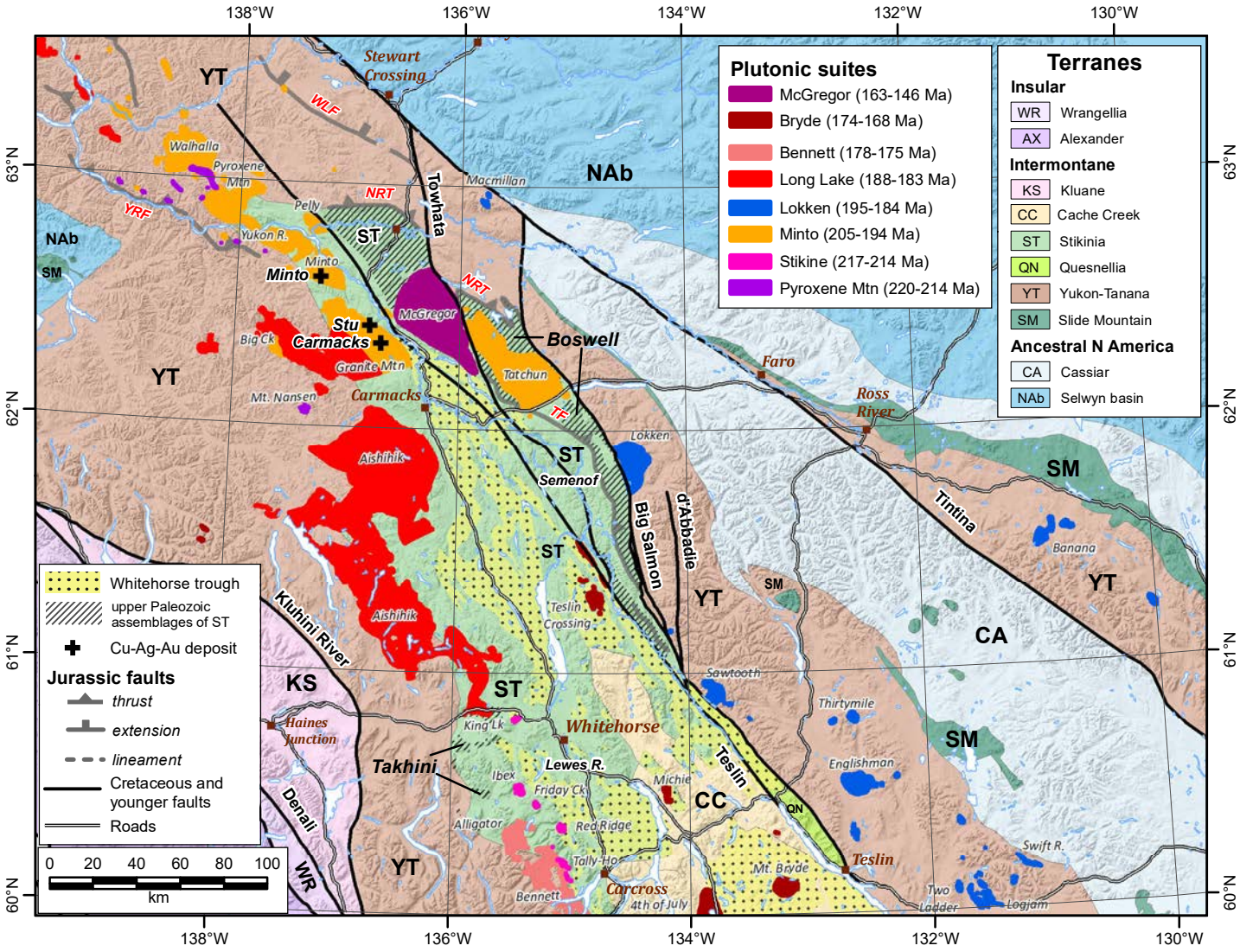
138°W
136°W
134°W
132°W
130°W
63°N
62°N
61°N
60°N
Plutonic suites
McGregor (163-146 Ma)
Bryde (174-168 Ma)
Bennett (178-175 Ma)
Long Lake (188-183 Ma)
Lokken (195-184 Ma)
Minto (205-194 Ma)
Stikine (217-214 Ma)
Pyroxene Mtn (220-214 Ma)
Terranes
Insular
WR Wrangellia
AX Alexander
Intermontane
KS Kluane
CC Cache Creek
ST Stikinia
QN Quesnellia
YT Yukon-Tanana
SM Slide Mountain
Ancestral N America
CA Cassiar
NAb Selwyn basin
Whitehorse trough
upper Paleozoic assemblages of ST
Cu-Ag-Au deposit
Jurassic faults
thrust
extension
lineament
Cretaceous and younger faults
Roads
0 20 40 60 80 100
km
Stewart Crossing
WLF
Walhalla
Pyroxene Mtn
YRF
Pelly
NRT
Yukon R.
Minto
Macmillan
Towhata
Minto
Stu
Carmacks
Big Ck
Granite Mtn
Mt. Nansen
McGregor
Boswell
Tatchun
Carmacks
Faro
Ross River
TF
Lokken
Semenof
Aishihik
Big Salmon
d'Abbadie
Tintina
Banana
Kluhini River
Teslin Crossing
Sawtooth
Thirtymile
Haines Junction
King Lk
Whitehorse
Takhini
Ibex
Lewes R.
Friday Ck
Michie
Teslin
Englishman
Denali
Alligator
Red Ridge
Tally-Ho
Mt. Bryde
Swift R.
Bennett
Carcross
4th of July
Two Ladder
Logjam
YT
NAb
SM
ST
KS
CC
QN
WR
CA

Figure 3.

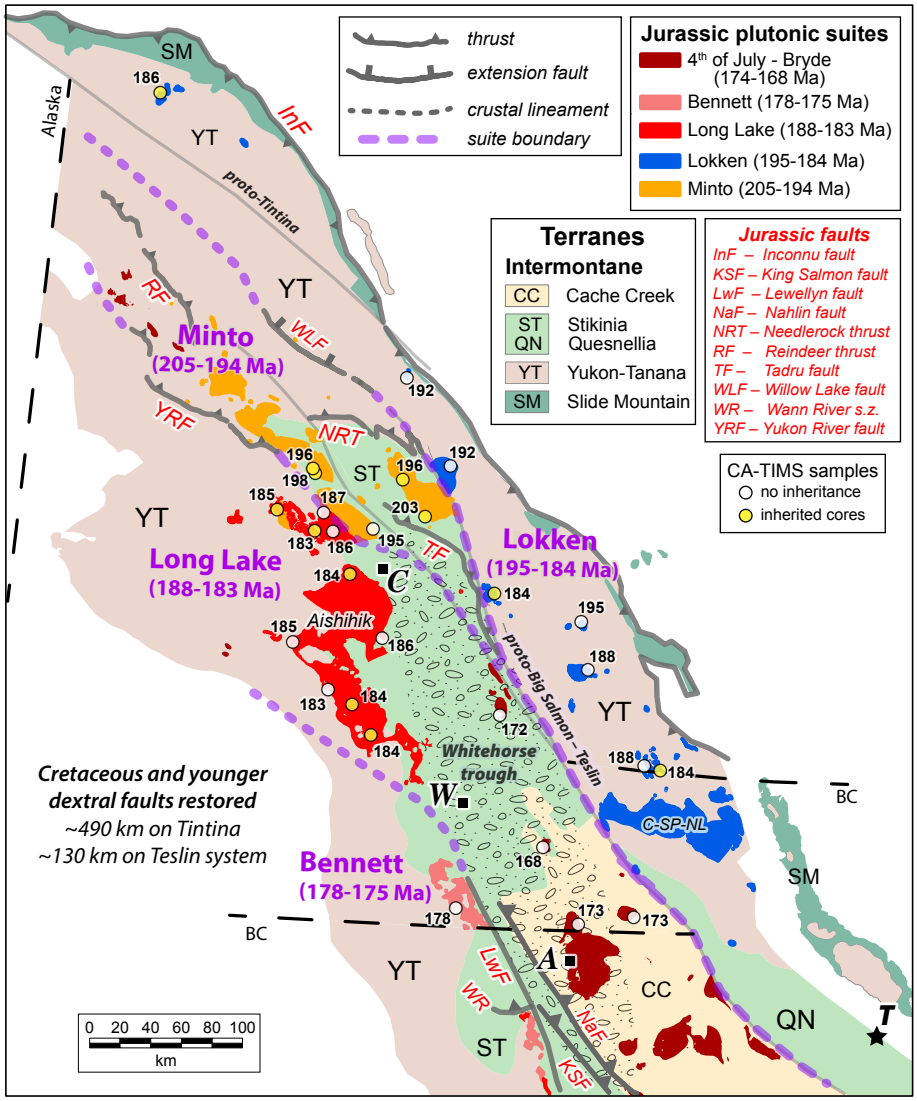
thrust
extension fault
crustal lineament
suite boundary
Jurassic plutonic suites
4th of July - Bryde (174-168 Ma)
Bennett (178-175 Ma)
Long Lake (188-183 Ma)
Lokken (195-184 Ma)
Minto (205-194 Ma)
Terranes
Intermontane
CC Cache Creek
ST Stikinia
QN Quesnellia
YT Yukon-Tanana
SM Slide Mountain
Jurassic faults
InF – Inconnu fault
KSF – King Salmon fault
LwF – Lewellyn fault
NaF – Nahlin fault
NRT – Needlerock thrust
RF – Reindeer thrust
TF – Tadru fault
WLF – Willow Lake fault
WR – Wann River s.z.
YRF – Yukon River fault
CA-TIMS samples
no inheritance
inherited cores
Alaska
SM
YT
ST
QN
CC
BC
InF
proto-Tintina
RF
WLF
YRF
NRT
TF
Minto (205-194 Ma)
Long Lake (188-183 Ma)
Lokken (195-184 Ma)
Aishihik
Whitehorse trough
proto-Big Salmon – Teslin
C-SP-NL
Bennett (178-175 Ma)
LwF
WR
NaF
KSF
C
A
W
T
Cretaceous and younger dextral faults restored
~490 km on Tintina
~130 km on Teslin system
0 20 40 60 80 100
km

Figure 4.

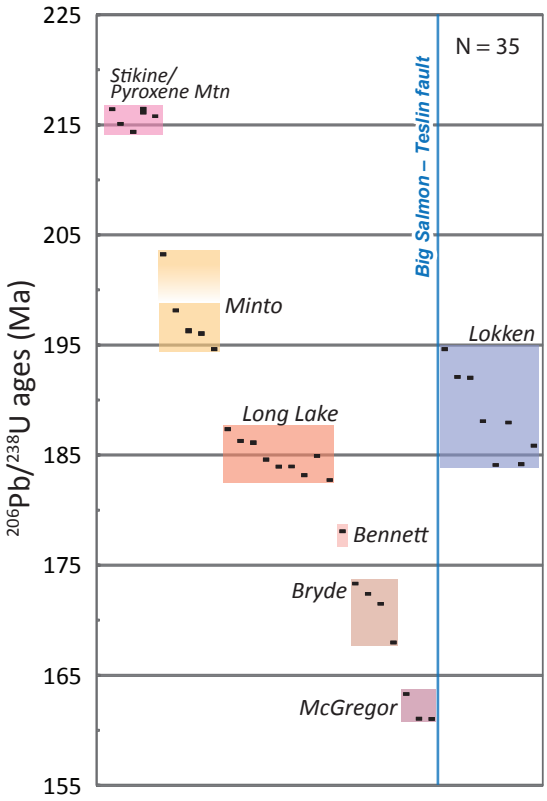
225
215
205
195
185
175
165
155
$^{206}Pb/^{238}U$ ages (Ma)
N = 35
Big Salmon – Teslin fault
Stikine/
Pyroxene Mtn
Minto
Lokken
Long Lake
Bennett
Bryde
McGregor

Figure 5.

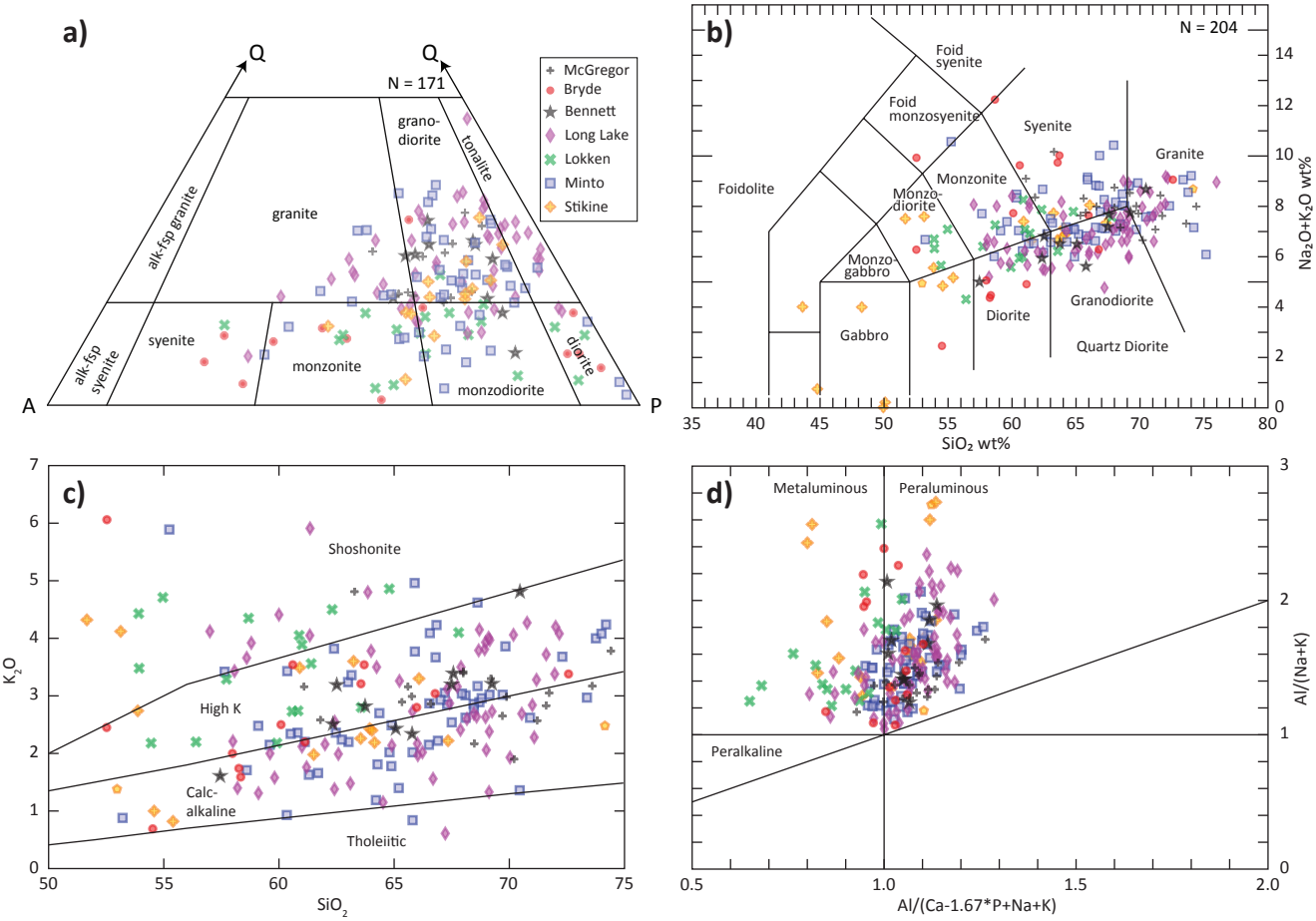
a)
Q
Q
N = 171
grano-
diorite
tonalite
granite
alk-fsp granite
alk-fsp
syenite
syenite
monzonite
monzodiorite
diorite
A
P
McGregor
Bryde
Bennett
Long Lake
Lokken
Minto
Stikine
b)
N = 204
Foid
syenite
Foid
monzosyenite
Syenite
Granite
Foidolite
Monzonite
Monzo-
diorite
Monzo-
gabbro
Granodiorite
Diorite
Gabbro
Quartz Diorite
Na_2O+K_2O wt%
SiO_2 wt%
c)
Shoshonite
High K
Calc-
alkaline
Tholeiitic
K_2O
SiO_2
d)
Metaluminous
Peraluminous
Peralkaline
Al/(Na+K)
Al/(Ca-1.67*P+Na+K)

Figure 6.

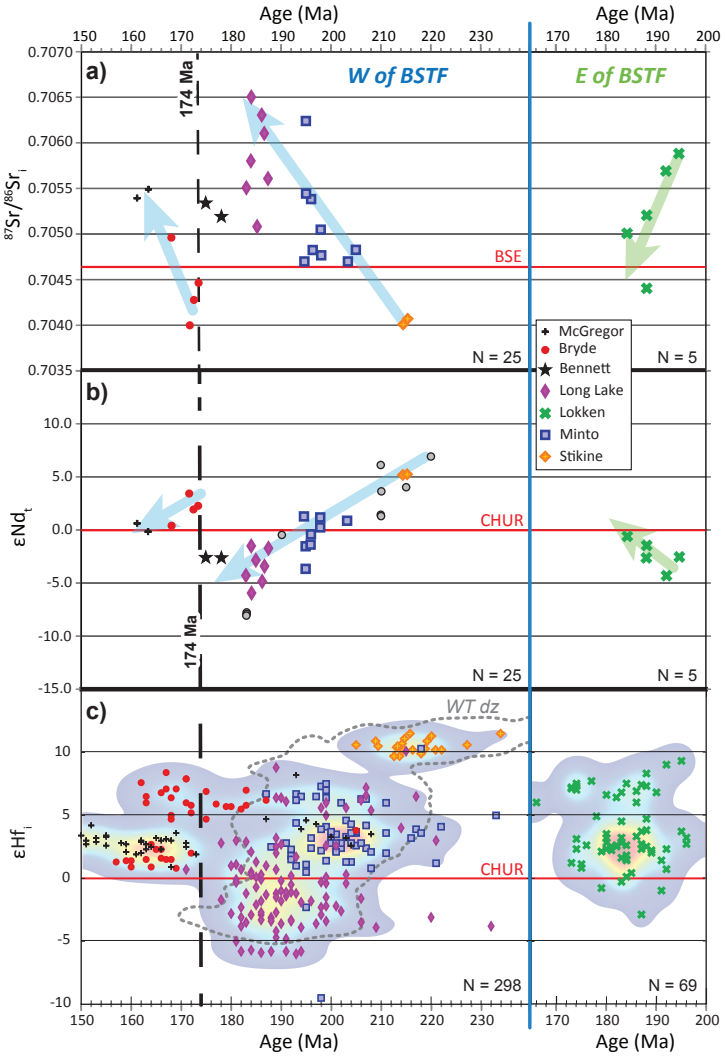
Age (Ma)
Age (Ma)
a)
W of BSTF
E of BSTF
174 Ma
BSE
N = 25
N = 5
McGregor
Bryde
Bennett
Long Lake
Lokken
Minto
Stikine
b)
CHUR
174 Ma
N = 25
N = 5
c)
WT dz
CHUR
N = 298
N = 69
Age (Ma)
Age (Ma)

Figure 7.

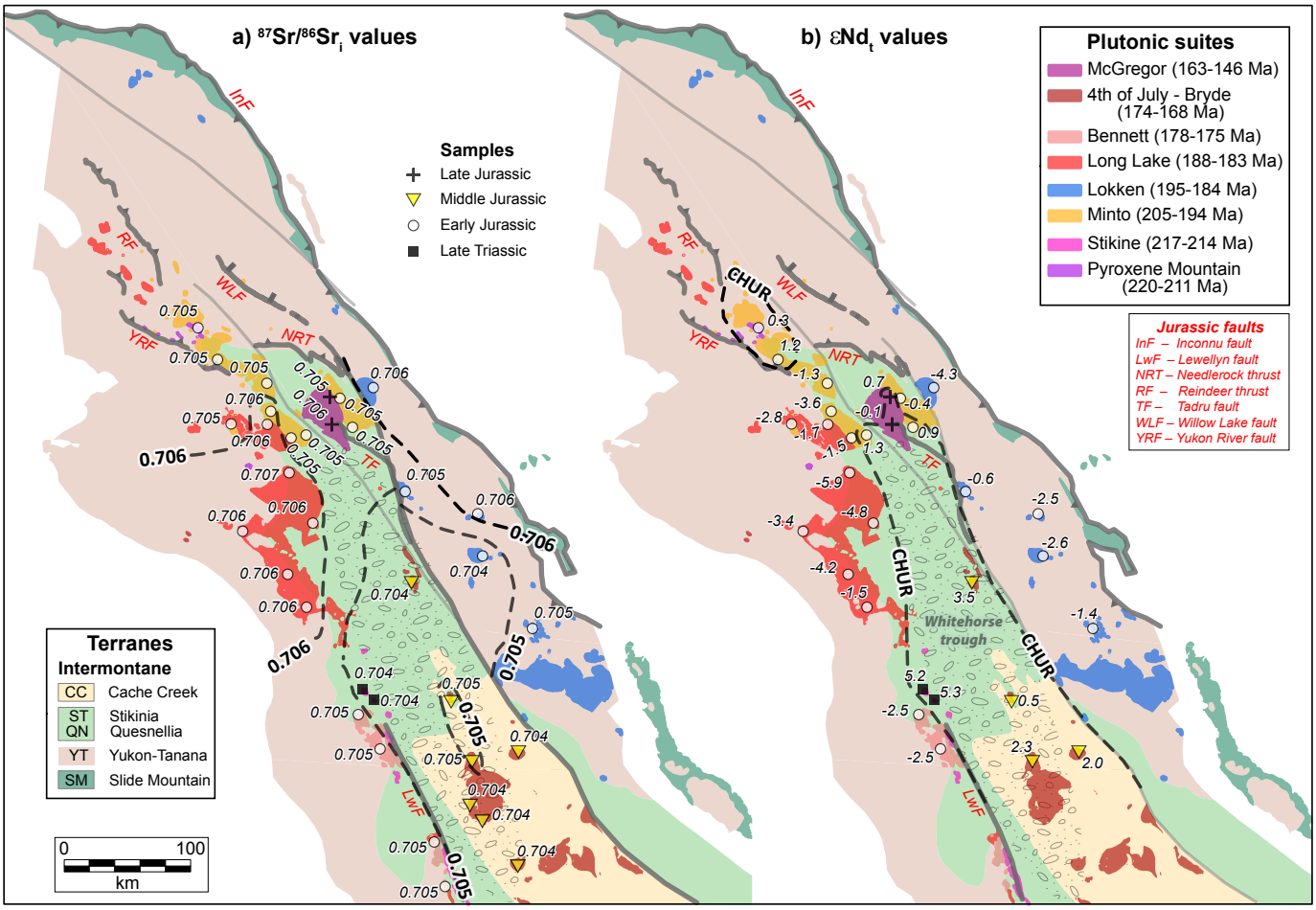
a) $^{87}Sr/^{86}Sr_i$ values
b) εNd_t values
Samples
Late Jurassic
Middle Jurassic
Early Jurassic
Late Triassic
Plutonic suites
McGregor (163-146 Ma)
4th of July - Bryde (174-168 Ma)
Bennett (178-175 Ma)
Long Lake (188-183 Ma)
Lokken (195-184 Ma)
Minto (205-194 Ma)
Stikine (217-214 Ma)
Pyroxene Mountain (220-211 Ma)
Jurassic faults
InF – Inconnu fault
LwF – Lewellyn fault
NRT – Needlerock thrust
RF – Reindeer thrust
TF – Tadru fault
WLF – Willow Lake fault
YRF – Yukon River fault
Terranes
Intermontane
CC Cache Creek
ST QN Stikinia Quesnellia
YT Yukon-Tanana
SM Slide Mountain
0 100 km
CHUR
Whitehorse trough

Figure 8.

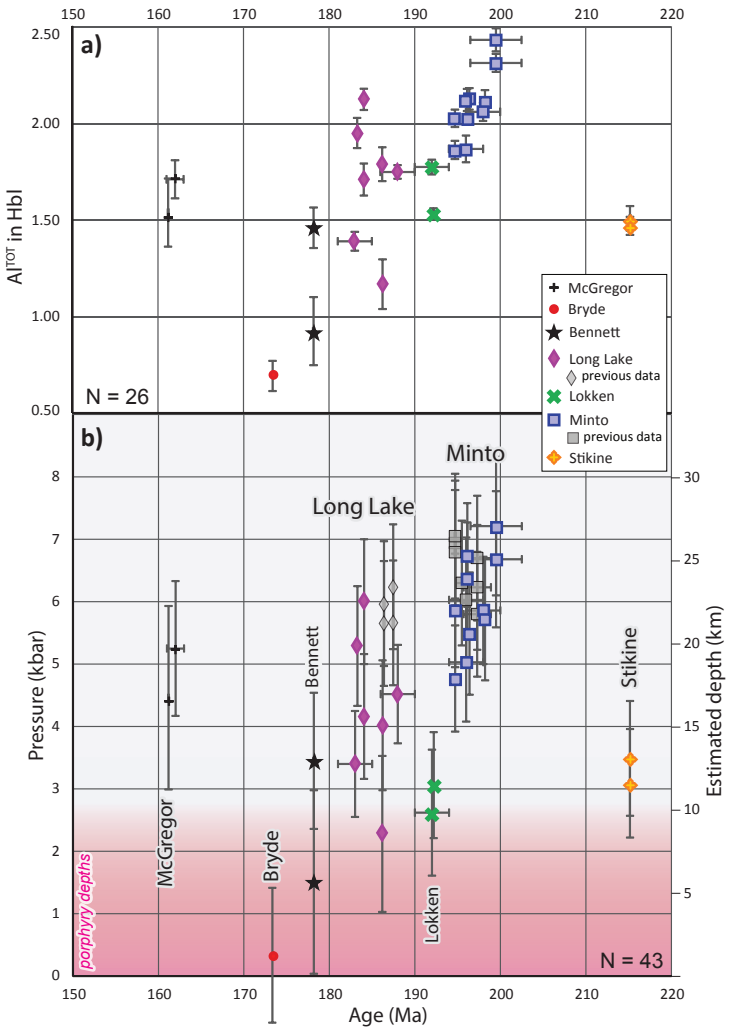
a)
b)
N = 26
N = 43
Al^{TOT} in Hbl
Pressure (kbar)
Estimated depth (km)
Age (Ma)
McGregor
Bryde
Bennett
Long Lake
previous data
Lokken
Minto
previous data
Stikine
porphyry depths

Figure 9.

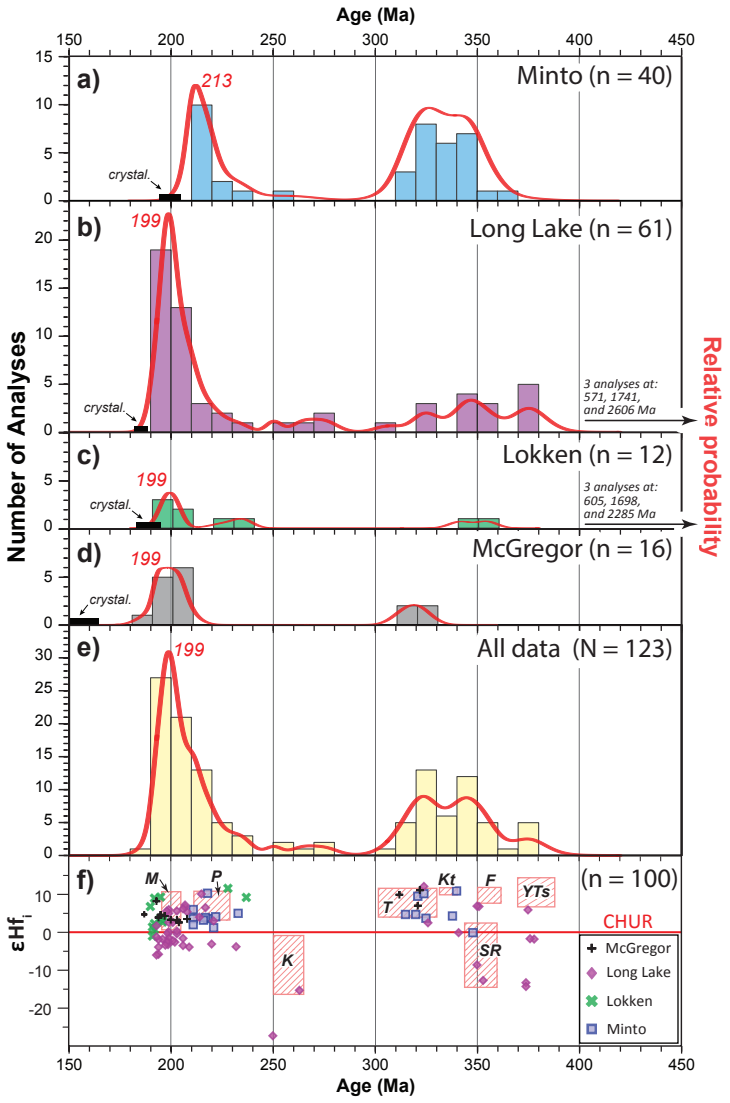
Age (Ma)
a)
Minto (n = 40)
213
crystal.
b)
Long Lake (n = 61)
199
crystal.
3 analyses at:
571, 1741,
and 2606 Ma
c)
Lokken (n = 12)
199
crystal.
3 analyses at:
605, 1698,
and 2285 Ma
d)
McGregor (n = 16)
199
crystal.
e)
All data (N = 123)
199
f)
(n = 100)
M
P
K
T
Kt
F
YTs
SR
CHUR
McGregor
Long Lake
Lokken
Minto
Number of Analyses
Relative probability
εHf$_i$
Age (Ma)

Figure 10.

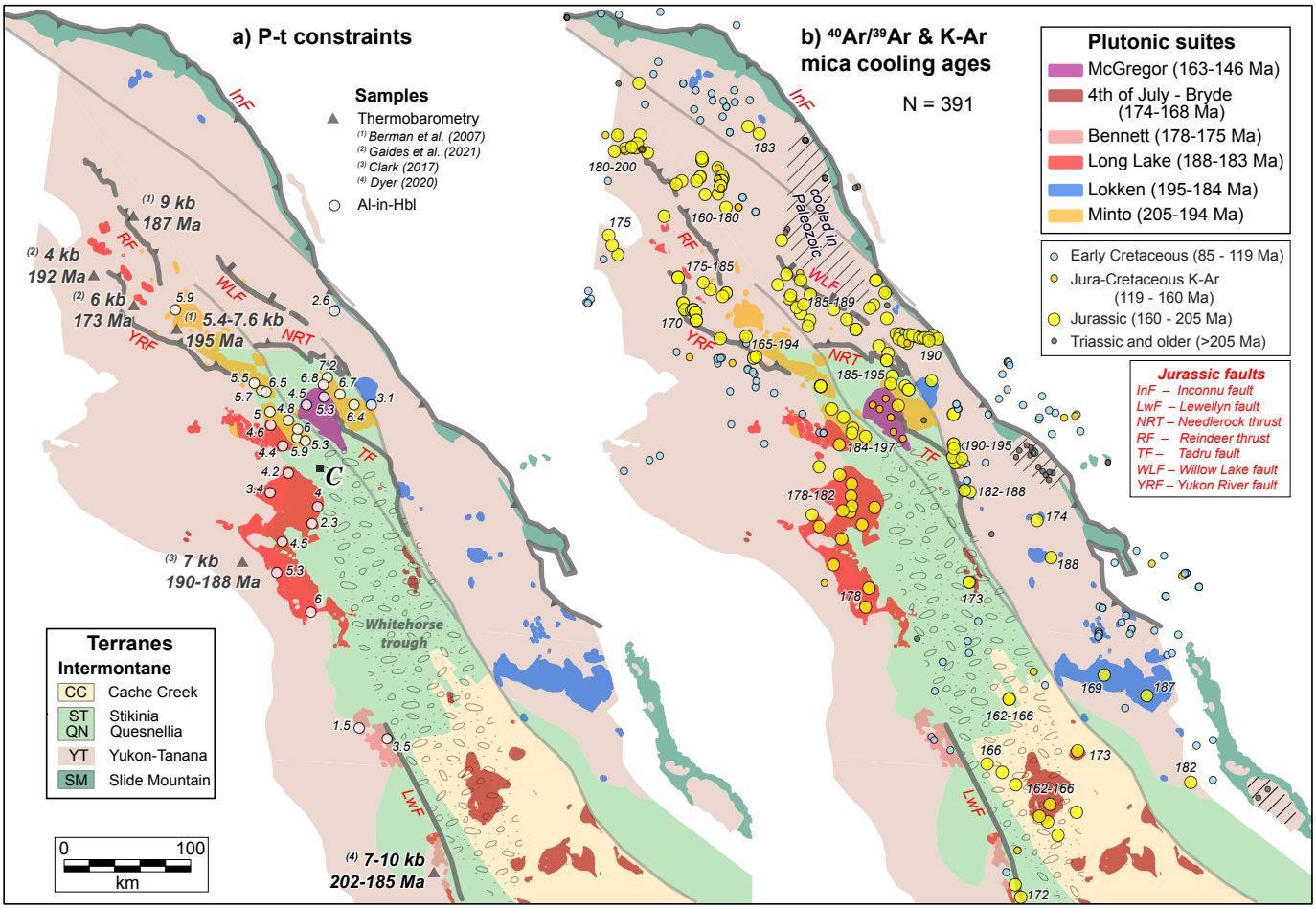
a) P-t constraints
b) 40Ar/39Ar & K-Ar mica cooling ages
N = 391
Samples
Thermobarometry
(1) Berman et al. (2007)
(2) Gaides et al. (2021)
(3) Clark (2017)
(4) Dyer (2020)
Al-in-Hbl
(1) 9 kb
187 Ma
(2) 4 kb
192 Ma
(2) 6 kb
173 Ma
(1) 5.4-7.6 kb
195 Ma
(3) 7 kb
190-188 Ma
(4) 7-10 kb
202-185 Ma
InF
RF
WLF
YRF
NRT
TF
LwF
Whitehorse trough
C
Terranes
Intermontane
CC Cache Creek
ST QN Stikinia Quesnellia
YT Yukon-Tanana
SM Slide Mountain
0
100
km
Plutonic suites
McGregor (163-146 Ma)
4th of July - Bryde (174-168 Ma)
Bennett (178-175 Ma)
Long Lake (188-183 Ma)
Lokken (195-184 Ma)
Minto (205-194 Ma)
Early Cretaceous (85 - 119 Ma)
Jura-Cretaceous K-Ar (119 - 160 Ma)
Jurassic (160 - 205 Ma)
Triassic and older (>205 Ma)
Jurassic faults
InF – Inconnu fault
LwF – Lewellyn fault
NRT – Needlerock thrust
RF – Reindeer thrust
TF – Tadru fault
WLF – Willow Lake fault
YRF – Yukon River fault
cooled in Paleozoic
180-200
183
175
160-180
175-185
170
165-194
185-189
190
185-195
184-197
178-182
190-195
182-188
174
188
178
173
169
187
162-166
166
173
182
162-166
172

Figure 11.

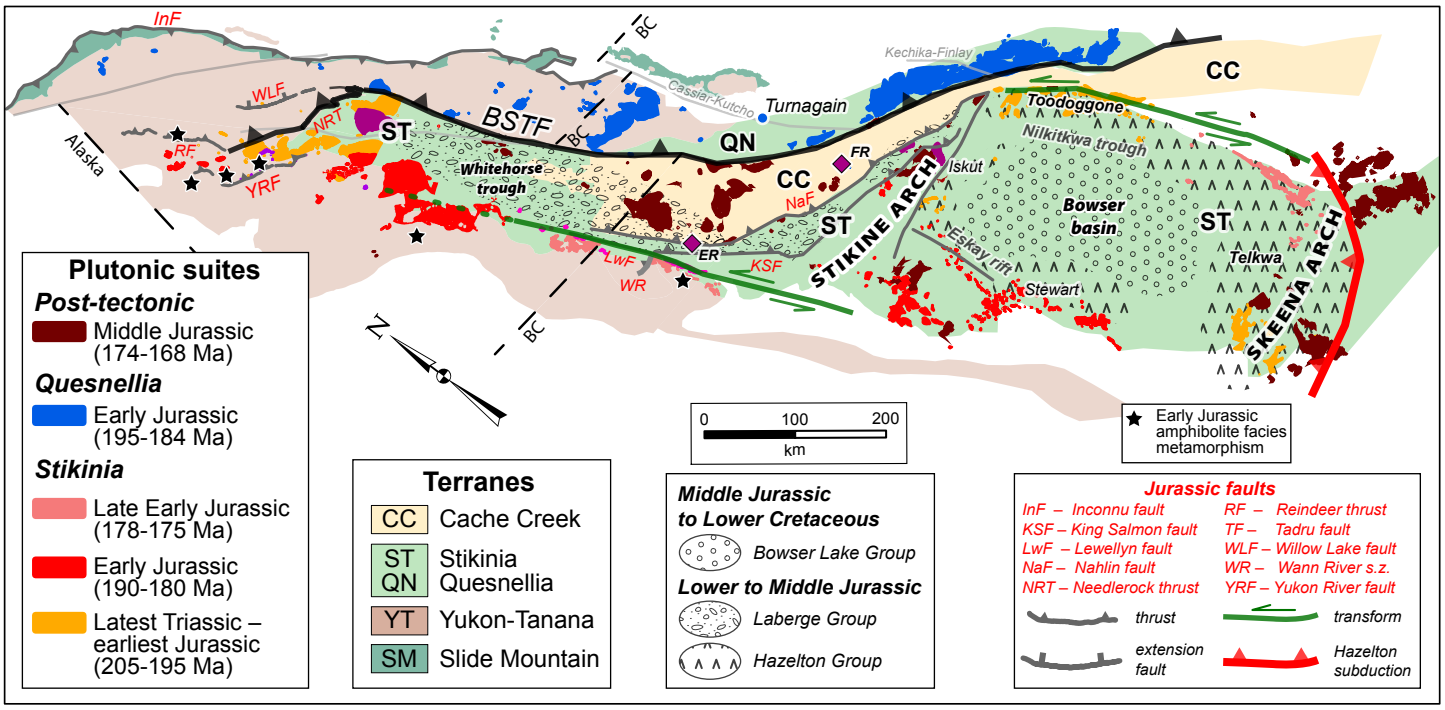
InF
WLF
NRT
RF
YRF
Alaska
BSTF
ST
Whitehorse trough
BC
Cassiar-Kutcho
Turnagain
Kechika-Finlay
QN
CC
FR
NaF
ER
KSF
LwF
WR
STIKINE ARCH
Eskay rift
Iskut
Stewart
Toodoggone
Nilkitkwa trough
Bowser basin
Telkwa
SKEENA ARCH
N
Plutonic suites
Post-tectonic
Middle Jurassic (174-168 Ma)
Quesnellia
Early Jurassic (195-184 Ma)
Stikinia
Late Early Jurassic (178-175 Ma)
Early Jurassic (190-180 Ma)
Latest Triassic – earliest Jurassic (205-195 Ma)
Terranes
CC Cache Creek
ST Stikinia
QN Quesnellia
YT Yukon-Tanana
SM Slide Mountain
0 100 200
km
Middle Jurassic to Lower Cretaceous
Bowser Lake Group
Lower to Middle Jurassic
Laberge Group
Hazelton Group
Early Jurassic amphibolite facies metamorphism
Jurassic faults
InF – Inconnu fault
KSF – King Salmon fault
LwF – Lewellyn fault
NaF – Nahlin fault
NRT – Needlerock thrust
RF – Reindeer thrust
TF – Tadru fault
WLF – Willow Lake fault
WR – Wann River s.z.
YRF – Yukon River fault
thrust
transform
extension fault
Hazelton subduction

Figure 12.

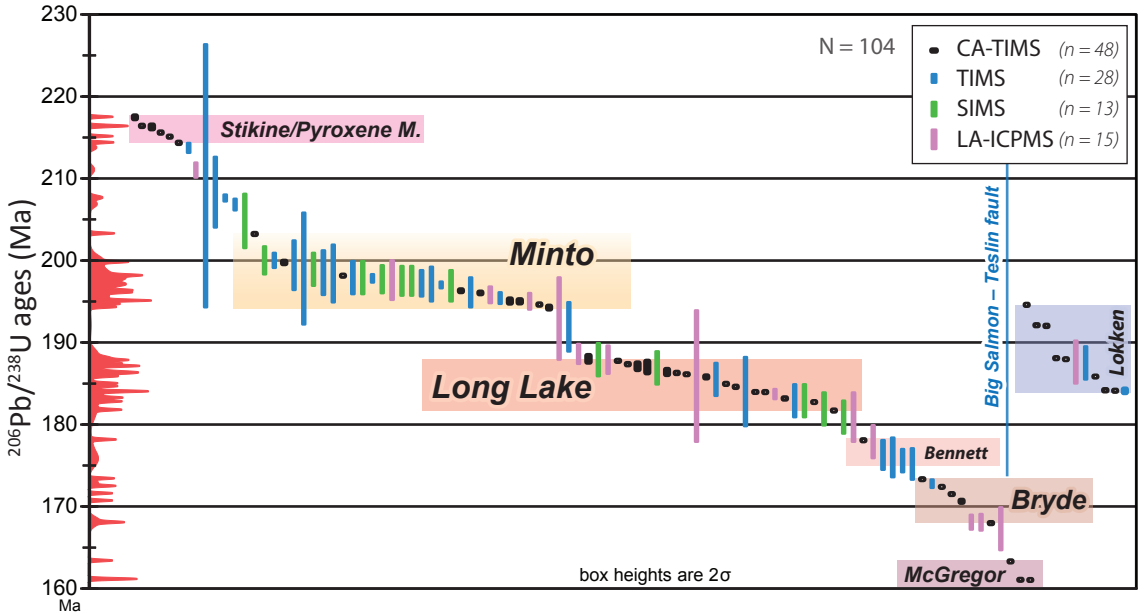
N = 104
CA-TIMS (n = 48)
TIMS (n = 28)
SIMS (n = 13)
LA-ICPMS (n = 15)
Stikine/Pyroxene M.
Minto
Long Lake
Bennett
Bryde
McGregor
Lokken
Big Salmon – Teslin fault
box heights are 2σ
$^{206}Pb/^{238}U$ ages (Ma)
230
220
210
200
190
180
170
160
Ma

Figure 13.

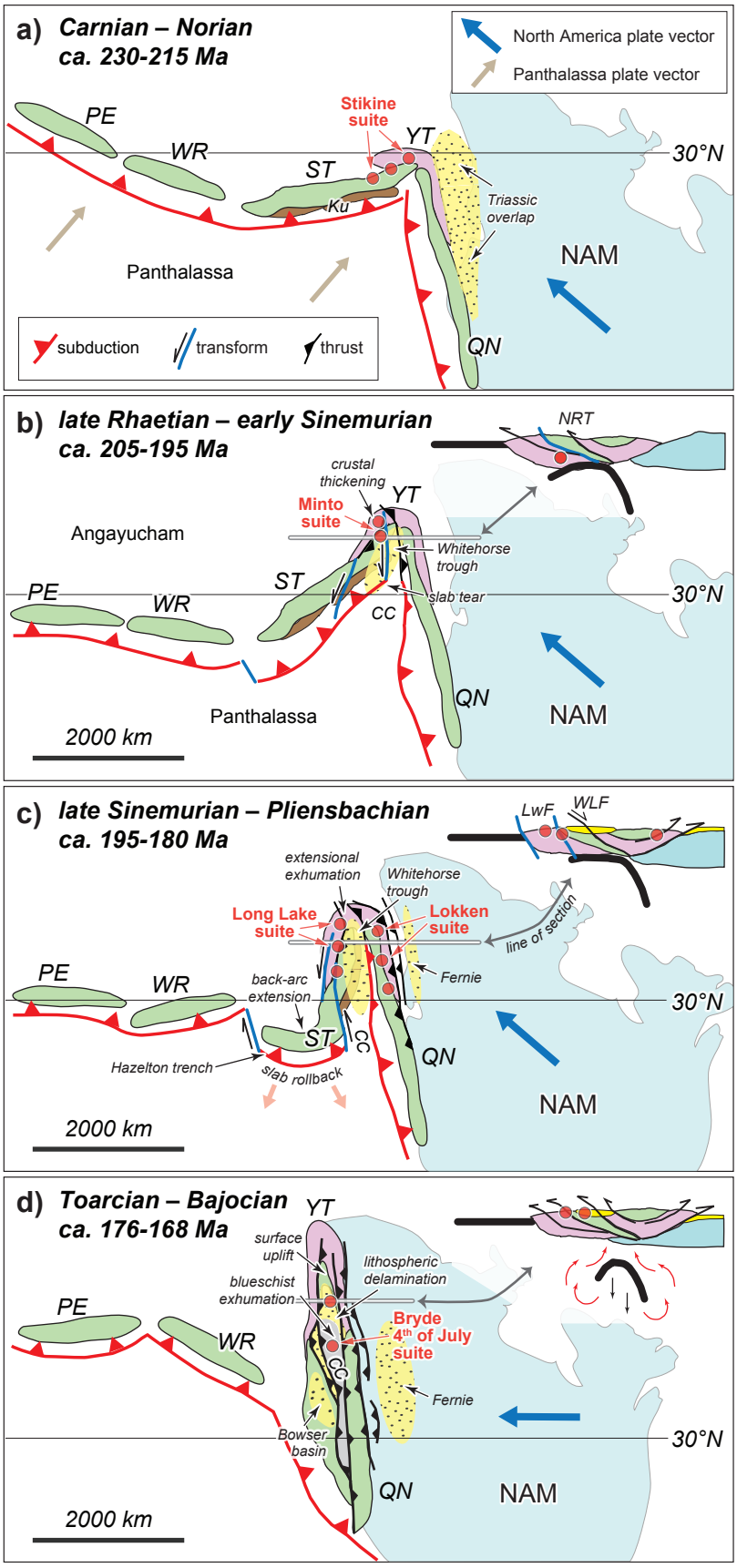
a) Carnian – Norian
ca. 230-215 Ma
North America plate vector
Panthalassa plate vector
PE
WR
Stikine suite
YT
ST
Ku
30°N
Triassic overlap
NAM
Panthalassa
subduction
transform
thrust
QN
b) late Rhaetian – early Sinemurian
ca. 205-195 Ma
NRT
crustal thickening
YT
Minto suite
Angayucham
Whitehorse trough
ST
PE
WR
slab tear
CC
30°N
QN
NAM
Panthalassa
2000 km
c) late Sinemurian – Pliensbachian
ca. 195-180 Ma
LwF
WLF
extensional exhumation
Whitehorse trough
Long Lake suite
Lokken suite
line of section
PE
WR
back-arc extension
Fernie
30°N
ST
CC
QN
Hazelton trench
slab rollback
NAM
2000 km
d) Toarcian – Bajocian
ca. 176-168 Ma
YT
surface uplift
lithospheric delamination
blueschist exhumation
PE
WR
Bryde 4th of July suite
CC
Fernie
30°N
Bowser basin
QN
NAM
2000 km